Numerical and Experimental Investigations of Oil Jet Cooling of Pistons

A Thesis Submitted
in
Partial Fulfillment of the Requirements
for the degree of

Master of Technology

by

MANI BIJOY VARGHESE

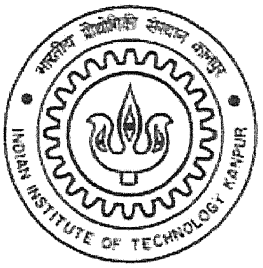

DEPARTMENT OF MECHANICAL ENGINEERING
INDIAN INSTITUTE OF TECHNOLOGY KANPUR

July, 2004

Numerical and Experimental Investigations of Oil Jet Cooling of Pistons

A Thesis Submitted
in
Partial Fulfillment of the Requirements
for the degree of

Master of Technology

by

MANI BIJOY VARGHESE

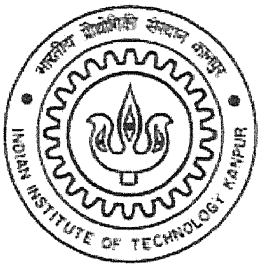

DEPARTMENT OF MECHANICAL ENGINEERING
INDIAN INSTITUTE OF TECHNOLOGY KANPUR

July, 2004

CERTIFICATE

It is certified that the work contained in the thesis entitled "Numerical and Experimental Investigations of Oil Jet Cooling of Pistons" by Mani Bijoy Varghese (Y210518) has been carried out under my supervision and this work has not been submitted elsewhere for the award of degree.

Dr. Avinash Kumar Agarwal
Assistant Professor
Department of Mechanical Engineering
Indian Institute of Technology Kanpur

Acknowledgements

With immense pleasure I express my sincere gratitude, regards and thanks to my supervisor Dr. Avinash Kumar Agarwal for his excellent guidance, invaluable suggestions and continous encouragement at all the stages of my research work. His interest and confidence in me was the reason for all the success I have made. I have been fortunate to have him as my guide as he has been a great influence on me, both as a person and as a professional.

I am extremely thankful to Prof. P. S. Ghoshdastidar, Department of Mechanical Engineering, IIT Kanpur and Prof. C. P. Garner, University of Loughborough, UK for their suggestions and support.

It was a pleasure to be associated with Energy Conversion Lab of IIT Kanpur, and I would like to thank all the staff members and my co-workers Sinhaji, Dhananjay, Mrityunjay, Shrawan, Sumit, Deepak and Sandeep. Special thanks to Pathakji, Raisji and Mohanlal, who were at some or the other point involved in my experimental set up. Last but not least I would like to thank Lalta Prasad, who had been of immense help to me, who despite his fragile health was always willing to help me in moving things.

I would like to thank my friends Abhijit, Amit, Anupam, Anoop, Deepak, Kisun, Prasad, Prince, Soumya, Sudhish, Santanu, Santosh and all my classmates for their smiles and friendship making the life at IIT Kanpur enjoyable and memorable.

Above all, I am blessed with such caring parents. I extend my deepest gratitude to my parents and my younger sister for their invaluable love, affection, encouragement and support.

Mani Bijoy Varghese

Abstract

Thermal loading of diesel engine pistons has increased dramatically in recent years due to applications of various advanced technologies to meet low emission and high power requirements. Control of piston temperatures by cooling of pistons has become one of the determining factors in a successful engine design. The pistons are cooled by oil jets fired at the underside from the crankcase. Any undesirable piston temperature rise may lead to engine seizure because of piston warping/deformation. However, if the temperature at the underside of the piston, where oil jet strikes the piston, is above the boiling point of the oil being used, it may contribute to the mist generation in the crankcase. This mist may significantly contribute to the non-tail pipe emisssions in the form of unburnt hydrocarbons (UBHC's), which has unfortunately not been looked into so seriously, as the current stress of all the automobile manufacturers is on meeting the tail pipe emission legislative limits.

In this investigation, a numerical model has been developed using finite elements method for studying the oil jet cooling of pistons. Using the numerical modeling, heat transfer coefficient (h) at the underside of the piston is predicted. This predicted value of heat transfer coefficient significantly helps in selecting right oil type, oil jet velocity, oil jet diameter and distance of the nozzle from the underside of the piston. It also helps predict whether the selected grade of oil will contribute to mist generation. Experimental validation of the numerical modeling were carried out on a flat plate. Problem of mist generation was also investigated on a flat plate using a web camera with frame speed of 15 fps.

Contents

List of Figures

List of Tables

List of Symbols

C_p	=	Specific heat of the oil, J/kgK
d	=	Nozzle diameter, m
D	=	Diameter of the disk, m
h	=	Local heat transfer coefficient at the bottom surface of the disk, W/m^2K
k_{jet}	=	Thermal conductivity of the oil jet, W/mk
k_r	=	Thermal conductivity of the material in r direction
k_z	=	Thermal conductivity of the material in z direction
Nu	=	Local Nusselt number = $\frac{hD}{k_{jet}}$
Nu_0	=	Stagnation Point Nusselt number
Pr	=	Prandtl number of the oil jet = $\frac{\mu C_p}{k_{jet}}$
r	=	Distance from the left hand side of the piston center
Re	=	Jet Reynolds number based on the nozzle diameter = $\frac{vd}{\nu}$
v	=	$v_{jet(absolute)}$ - v_{piston} = relative jet velocity (averaged over a cycle), m/s
w	=	Weight function
z	=	Distance from the underside of the piston
z_0	=	Vertical distance of the disk from the nozzle exit, m
ν	=	Kinematic viscosity of the oil, m^2/s
μ	=	Dynamic viscosity of the oil, kg/ms
$\psi_j(r,z)$	=	Shape function

Chapter 1

Introduction

Direct Injection (DI) diesel engines have an advantage in fuel economy compared to gasoline engines. Diesel engines are eco-friendly and have good potential to meet future exhaust emission regulations because of the lower carbondioxide (CO_2) emissions. Diesel engines however suffer from the problem of emission of nitrogen oxides (NO_x) and particulate matter (PM). Requirements of higher power, lower engine weight, volume and lower fuel consumption are the main requirements in case of diesel engines installed on commercial vehicles such as trucks and buses. In order to meet these requirements, current diesel engines are required to have boosted turbo-charging, high pressure fuel injection and improved airflow in piston combustion bowl. The current trend in the automobile industry is towards increasing the power density of the engines and making lighter engines. These requirements lead to higher thermal load on the engine, especially on the pistons. In the heavy duty diesel engines, combustion chamber and cylinder head are normally water cooled. The piston however cannot be cooled using water jacket because of logistics problem. The piston temperature is one of the limiting factors in high-powered internal combustion engines. This problem is particularly severe in transportation engines,

where the space-weight to power ratio is of prime importance. In this case, the bore and stroke have to be kept to a minimum and the engine speed is limited by piston velocity. The only factor, which can be improved, is the mean cylinder pressure. An increase in mean cylinder pressure necessarily means additional heat input to the cylinder, a part of which has to be rejected through the walls of the combustion chamber and piston. Thus, the increase in density of the heat flux causes rise in cylinder wall and piston temperatures. The temperatures of certain critical areas in piston need to be kept low because of material constraints. Aluminum alloys begin to melt at temperatures greater than 500 ^{0}C as shown in figure 1.1 [1]. The liner and the cylinder head can be however be maintained at a reasonably high temperatures by suitably adjusting the water or air cooling. The valve temperatures can also be controlled by adequate cooling or air circulation through the engine.

Figure 1.1: Piston Scuffing Due to Excessive Piston Temperatures [2]

The total heat flow through the piston crown amounts to about 2 percent of the energy released by the fuel. The direct effect of the piston cooling on thermal efficiency of the engine is therefore miniscule. A large part of this heat loss represents heat transferred to the piston during the exhaust process; therefore the direct loss of what would otherwise be available energy is probably considerably

less than 1 percent of total heat input. Typical heat balance for the piston cooling load in a heavy duty diesel engine is given in table 1.1.

Heat Dissipation Location	Dissipation (percent)
Heat dissipation from undercrown surface	71
Heat dissipation from undercrown surface behind ring-groove pad	11
Heat dissipation from upper and lower skirt sections	10
Heat dissipation from rings and lands	8

Table 1.1: Heat Balance for Piston-Cooling Load [3]

The piston is usually cooled by oil jets fired to the underside from the crankcase in a heavy-duty diesel engine as shown in figure 1.2. The oil jets hit the hot piston at a very high relative velocity ranging from 5 m/s to 50 m/s. The oil jet breaks into mist because of high temperature at the underside of the piston and high relative velocity. This piston cooling generated mist contributes significantly towards the non-tail pipe emissions from the engine.

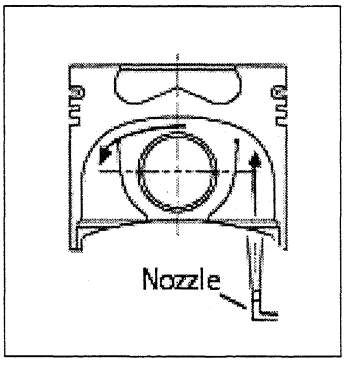

Figure 1.2: Oil Jet Cooled Piston

1.1 Methods of Piston Cooling

The piston can be cooled by oil, water or air. Water cooling was applied to heavy, low speed engines for some time; but more recently it is abandoned because of serious design and maintenance difficulties with piping and sealing. However, this type of cooling has advantages, since water has a higher specific heat and lower viscosity than oil and thus better heat transfer takes place.

Air cooling is simpler from design point of view, but lower specific heat per unit volume requires very large quantities of air to be supplied to the piston. This involves bulky pipes and ducts and an additional air compressor, which makes it less practical.

The usual method is oil cooling, in which oil can be supplied from the main lubrication system along the connecting rod to the piston or from a seperate oil supply. After piston cooling, the oil return to the crankcase. There are six different types of method of oil cooling of pistons.

1. In splash lubrication system, there is no direct oil supply to the piston. The oil retained in the crankcase is churned and splashed up by the internal parts of the engine (connecting rod big end and crankshaft) into a combination of liquid and mist. The oil mist is sprayed over the interior of the engine ie:- on the cylinder walls and on the underside of the piston crown. The heat from the piston inside is transferred to the crankcase atmosphere. This method is applied to engines having no forced lubrication of the small end of the connecting rod.

2. Cooling due to oil emerging from the small end bearings, which are pressure lubricated. Piston of marine engines are cooled with the help of pressure lubricated oil emerging from the small end bearings as shown in figure 1.3.

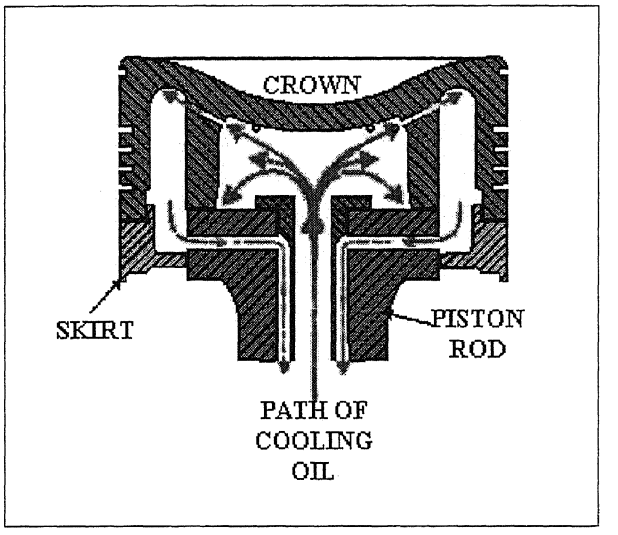

Figure 1.3: Piston Cooling with the help of Pressure Lubricated Oil Emerging from Small End Bearings [4]

3. The third method uses nozzle plate and nozzles as shown in figure 1.4. The oil goes up the annular space formed between the oil tube and the bore in the piston rod, and returns down the centre. The oil is sprayed up into the matching bores on the underside of the crown. This allows the crown to be made very thin as possible, in order to allow maximum heat transfer while maintaining strength.

4. "Cocktail shaker" is a cooling method applied particularly to engine pistons. The oil is brought into a closed chamber below the piston crown and released from the chamber to the crankcase through overflow holes or baffles. The overflow is arranged in such a manner that the volume of the chamber is only partly filled with oil. The oil is agitated violently by the piston reciprocating movement and the turbulence of the oil motion produces a high heat transfer coefficient between oil and the piston.

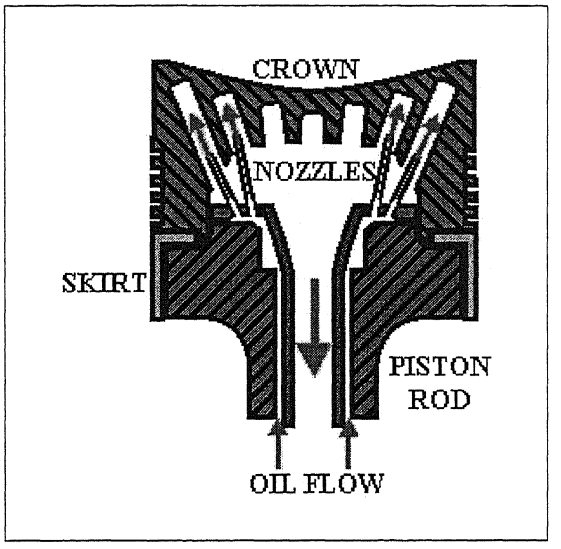

Figure 1.4: Piston Cooling Using Nozzles and Nozzle Plates [4]

5. Oil jet cooling, where the oil is released at high pressure from a nozzle mounted on the cylinder block and the nozzle directed towards the underside of the piston. The oil jet hits the undercrown of the piston and is then splashed on to the surrounding walls of the piston. Simple schematic of oil jet cooling is shown in figure 1.2. Jet cooling used in a heavy duty diesel engine (Elsbett make) is shown in figure 1.5.

6. The methods 4 and 5 are often combined, that is, the oil is injected from the top of the connecting rod onto the piston undercrown and then cooled in the "cocktail shaker" chamber from which it is released through the overflow to the crankcase.

Out of the six methods, oil jet cooling method is most practical for cooling of pistons and is used extensively in commercial heavy duty diesel engines.

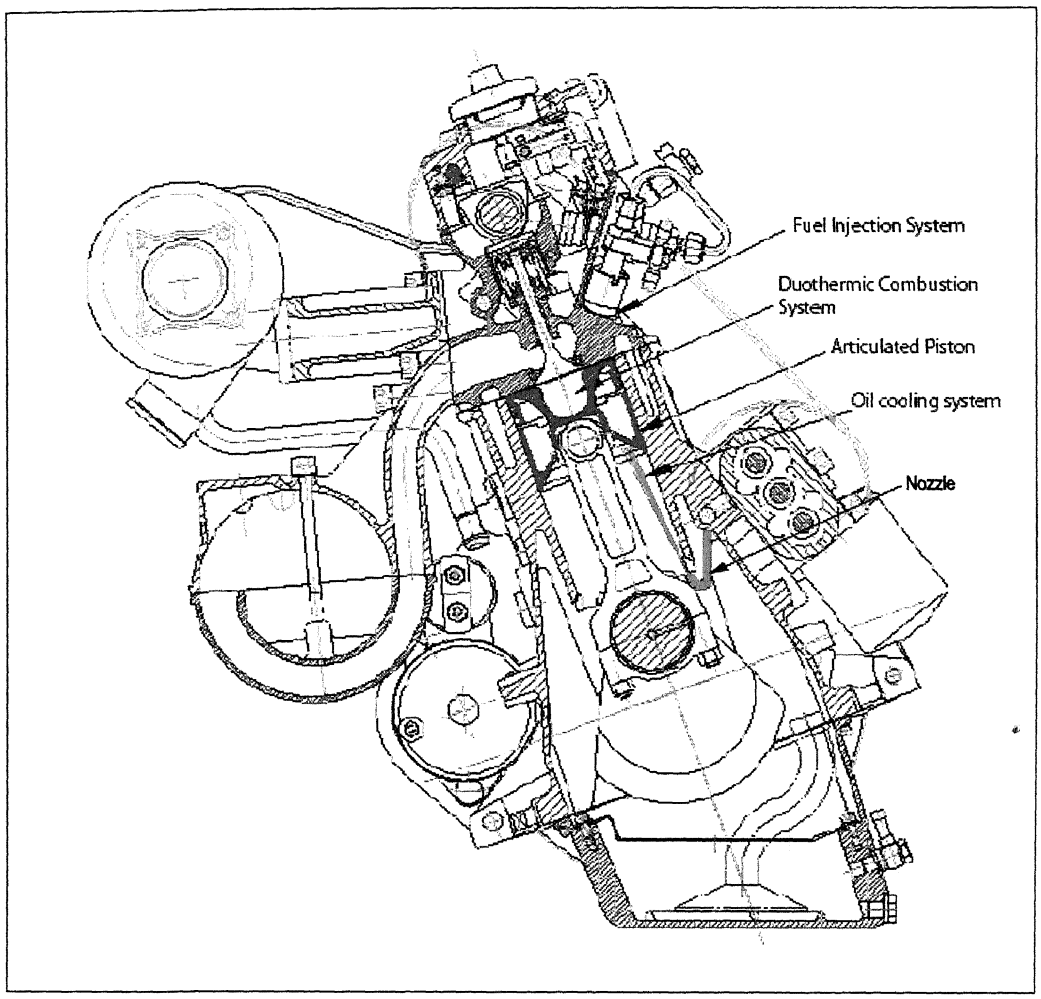

Figure 1.5: Cross-Sectional View of a Heavy Duty Diesel Engine Using an Oil Jet for Cooling of Piston [5]

1.2 Oil Jet Cooling of Pistons

The higher boosted turbo-charging enables the combustion in the high excess air region. Boosted turbo-charging is effective to reduce the NO_x and PM, and can realize high power and fuel economy from the engine. However, it causes increase in peak firing pressures and temperatures of the power cell parts (such as pistons, piston rings and cylinder liners). Therefore, it becomes difficult

to have sufficient reliability and durability when boosted turbo-charging is used. The increase in the piston temperature causes cavity edge cracking due to increase in thermal load and reduction in material strength. An excessive temperature of the piston results in piston scuffing, increased blow-by losses by sticking of the piston rings to the grooves and an increased oil consumption caused by wear of piston rings and ring grooves. These in turn decrease the reliability and durability of the engine significantly. Therefore, the control of piston temperature by piston cooling becomes important. There are two approaches to cope with the increase in thermal load of the pistons. One is improvement of piston cooling ability through redesigning of piston structure. The other is improvement of material strength in the high temperature region. The heat transfer coefficient in the cooling gallery has great effect on the piston temperature. However, it is hard to predict with sufficient accuracy because it is influenced by various factors, e.g: oil flow, engine speed, oil hole diameter etc. Figure 1.6 shows the structure of a oil jet cooled piston, which is generally used in heavy duty diesel engines. In this, cooling oil is sprayed from

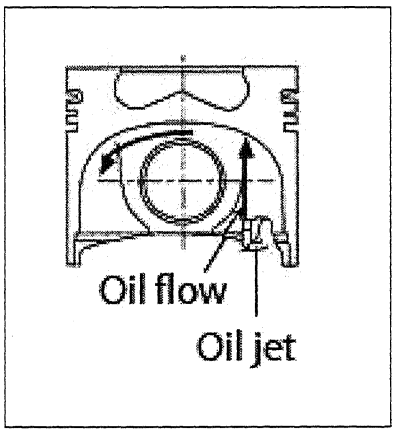

Figure 1.6: Oil Jet Cooling of Piston Without Cooling Gallery

an oil jet nozzle mounted on the lower deck of the cylinder block, to the backside

of the piston crown. There are no oil cooling galleries in this configuration. Figure 1.7 and 1.8 show the structure of a piston with cooling galleries, which has higher capacity of piston cooling than those without cooling gallery (figure 1.6). The latter

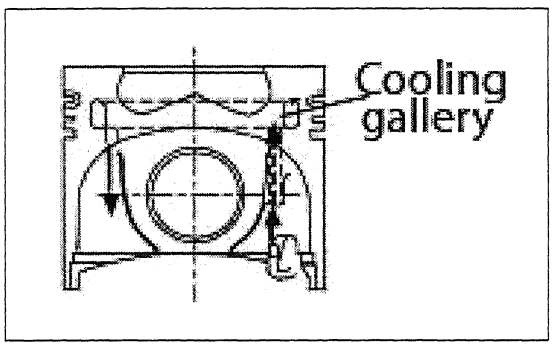

Figure 1.7: Oil Jet Cooling of Piston with Cooling Gallery (Salt-Core)

approach uses high strength materials in the high temperature region of a piston eg:- high strength aluninum alloys formed by changing the chemical ingredients, composites with ceramic fibres etc. In heavy-duty diesel engines, ferrous pistons,

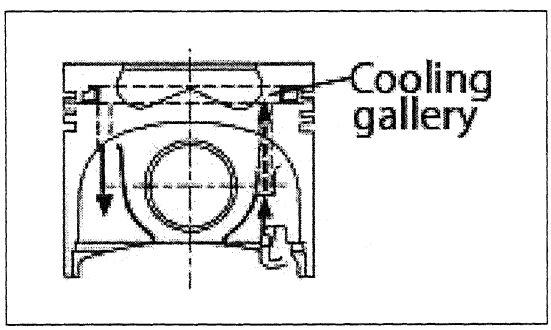

Figure 1.8: Oil Jet Cooling of Piston with Cooling Gallery (Hollow Ring Groove Insert)

which have higher strength than aluminum alloys are also used. Such examples include the articulated pistons, which combine a steel crown with an aluminum skirt, and the nodular cast iron mono-block pistons. Recently, articulated pistons came

into serial production for high speed, high output direct injection diesel engines. This piston configuration appears as today's most suitable design to withstand the new engine performance requirements. Articulated piston is shown in figure 1.9. Most of the state-of-art of piston cooling technique came out of the need to keep

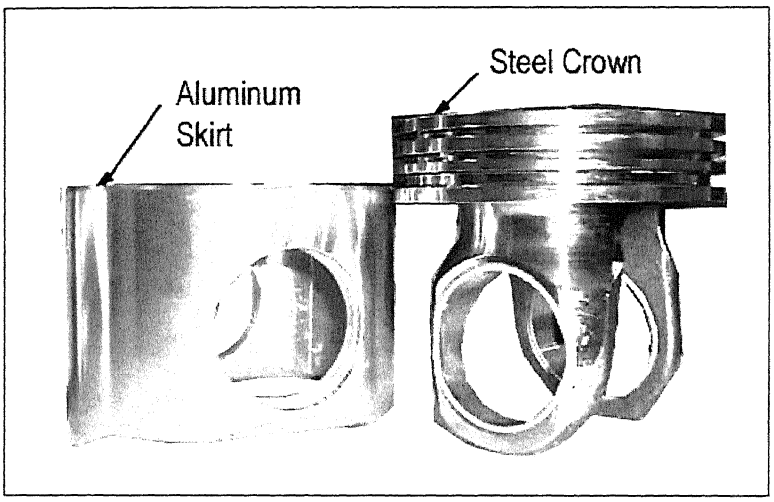

Figure 1.9: Articulated Piston

the aluminum pistons structurally suitable to resist the increasing engine power, as well as, to control the carbon buildup. This fact led piston manufacturers to develop appropriate inner designs suitable to improve piston-cooling conditions. Special nozzles are mounted on the engine block to throw cooler oil against the piston undercrown and to increase the heat exchange. Closed galleries are projected around the combustion bowl in order to remove heat and to decrease the combustion bowl rim and the ring groove zone temperature.

1.3 Objective of this Investigation

Heavy-duty diesel engine pistons are cooled by oil jet fired at the underside of the piston by a nozzle mounted on the cylinder block. The oil jet

breaks into mist because of high temperature at the underside of the piston and high relative velocity. This piston cooling generated mist contributes significantly towards the non-tail pipe emissions from the engine, which has unfortunately not been looked into seriously by automobile manufacturers. Brief objective of the current investigation is enumerated below.

1. Investigate the phenomenon of oil jet cooling of heavy-duty diesel engine piston.

2. Develop a numerical model for oil jet cooling of the piston. For this, the piston geometry need to be converted to a grid for Finite Element Analysis (FEA).

3. Select an appropriate heat transfer model to predict the piston temperature profile computationally.

4. Develop an experimental setup to perform the experiments on oil jet cooling of flat plate for validation of the computational model experimentally.

5. Investigate the conditions, under which the oil jet cooling of the piston start contributing significantly towards the non-tail pipe emissions through mist generation.

6. Extend this model to predict temperature distribution of heavy-duty diesel engine piston and effect of various parameters on cooling of piston.

Chapter 2

Literature Survey

The problem of air pollution created by automotive engines in metropolitan cities has become very severe and requires urgent corrective action. Unburnt hydrocarbons (UBHCs) are important pollutants, which are contributed by the following three sources in a petrol engine which is given in table 2.1.

Evaporative Losses	15 - 25%
Crankcase Blow-by	20 - 35%
Tailpipe Exhaust	50 - 60%

Table 2.1: Sources of UBHCs in a Petrol Engine [6]

In diesel engines, however, evaporative losses do not exist, crankcase blow-by is present but contribution made by it is not clearly known. It should be quite significant as pressures developed during combustion and power strokes are quite high. Also, in general, diesel engines are poorly maintained as compared to petrol engines. Most of the big engines are diesel powered therefore the contribution of hydrocarbon emission from diesel engines is quite large. The control of blow-by emissions is quite simple and inexpensive and results in 15-35% reduction in total UBHC emission together with increased lubricating oil change period and decreased

deterioration of lubricating oil. UBHC emissions from the diesel engines are mainly contributed by blow-by and the mist generated by oil jet cooling in modern high powered internal combustion engines. The oil jet cooling is an effective way of keeping the piston under-crown surface temperature under control.

2.1 Historical Perspective of Jet Cooling of Heated Surfaces

The studies of surface cooling by means of jets were originally conducted aiming the thermal protection of stator and rotor blades of gas turbines. Thus, extensive reviews presented in the literature such as by Martin (1977) refer to gas jets or air jet cooling in air surroundings [7]. Besides the problem of single jet, this study showed results with array of jets, discrete hole injection, and slot injection. Down and James (1987) presented experimental correlations for liquid jets in quiescent air [8]. They presented results from different works for many jet and flow conditions (Reynolds and Prandtl numbers), heating or cooling, liquid or gaseous medium, plane or concave surfaces, and circular array or slot jet. Hrycak (1988) presented studies on the impingement of round jets on flat and concave surfaces with models for turbine blades [9]. Beltaos (1976) analyzed the fluid dynamic behaviour of circular turbulent jet impingement [10]. Sparrow and Lovell (1980) obtained experimental data on jet impingement on surfaces at oblique angles (90^0-30^0) [11]. They observed that the point of maximum Nusselt number (Nu) moves upwards against the flow. However the mean value of the heat transfer coefficient (h) is not affected significantly.

Chang H. Oh et. al designed liquid jet array cooling modules for operation at very high load fluxes and used them to remove fluxes as high as 17 MW/m^2

[12]. The cooling was entirely covective without boiling. Wen et. al used impingement cooling on a flat surface by using circular jet with longitudinal swirl strips for cooling [13]. Smoke-flow visualization was used to investigate the behaviour of the complicated flow phenomenon under the swirling flow jet for this impingement cooling. Oliphant et. al compared liquid jet array and spray impingement cooling in the non-boiling regime experimentally [14]. Cornaro et. al used jet impingement cooling for convex semi-cylindrical surface [15].

Stevens and Webb experimentally investigated the effect of jet inclination on the local heat transfer coefficient on an obliquely impinging, round, free liquid jet striking a constant heat flux surface [16, 17]. The problem parameters investigated were jet Reynolds number in the range 6600 - 52000 and jet inclination ranging from 40 to 90 degree, measured from the horizontal. Experiments were carried out for nozzle sizes, d = 4.6 and 9.3 mm. It was found that the point of maximum heat transfer along the x-axis (the line of intersection of the jet inclination plane with the impingement surface) is shifted upstream (with respect to the jet flow) as a function of jet inclination with a maximum observed shift of 0.5 nozzle diameters. In addition, it was found that the shape of local Nusselt number profiles along the x-axis changed as the jet is inclined. One of the changes was the sharpening of the peak in the profile at the point of maximum heat transfer. Another change was an increasing asymmetry around the point of maximum heat transfer with the upstream side of the profile dropping off more rapidly than the downstream side.

2.2 Historical Perspective of Jet Cooling Applied to Engines

Studies on cooling of internal combustion engine started in 1960's. Bush and London introduced the term "cocktail shaker" [18]. Their interest was on reciprocating pistons with partially filled cavities. After long tests, heat transfer models and governing parameters were presented. Experimental correlations were obtained for liquids with Pr $>$ 0.5 and Pr $<<$ 1. The effect of piston reciprocating movement on the oil cooling gallery heat transfer coefficient was also analyzed by Bush and London [19], presenting basic design information for "cocktail shaker" cooled pistons. Advanced results were presented by French using different experimental rigs and engine test configurations and an expression for the heat transfer coefficient was presented [20]. Evans (1977) conducted a thorough study of the "cocktail shaker" piston cooling concept [21]. Movies of a flow visualization were taken using an open gallery. The main observation was the detection of different flow regimes in the off gallery. Considering the full 360^0 cycle of the piston (crank angle) six regimes were identified. Evans modeled these six regimes using known corelations and a numerical model was presented to evaluate the average value of h for each cycle.

Kajiwara et. al calculated the heat transfer coefficient in the cooling gallery of the oil jet cooled piston directly using CFD code [22]. Piston temperature distribution has also been predicted quite accurately using this approach. In order to realize the clean exhaust emission and the customer's requirements, such as higher power and fuel economy, one of the most effective designs in combustion bowl optimization is the re-entrant shape design. The active airflow and the lower thermal capacity working synerstically increase the bowl edge temperature. Therefore, it

becomes difficult to secure sufficient reliability and durability of the pistons that have the re-entrant combustion bowl.

Spray impingement cooling research is still being used to a great extent in acheiving high heat transfer rates from heating surfaces but are not being extensively used in automobiles currently.

Martins et. al (1993) analyzed the cooling conditions of articulated piston and their imapct on the piston performance in an effort to optimize articulated piston cooling [23]. Cooling conditions of articulated piston and their impact on the piston performance were analyzed. In order to evaluate the piston cooling optimization two configurations of cooling oil jet (single and double) were evaluated on a real time measuremnt test, together with two articulated piston skirt configuration (single and extended). The results showed the influence of engine valves location in the temperatures near the piston top and the influence of cooling oil jet in piston lower part temperatures. The results also showed the extended tray efficient behaviour in removing heat from piston undercrown when compared to double jet-single tray configuration.

Pimenta et. al used numerical simulation (finite element method) to study cooling of automotive pistons by liquid cooling jets [24]. Dhariwal investigated blow-by emission and lubricating oil consumption in an IC engine and tried to control blow-by losses using Positive Crankcase Ventilation (PCV) [6].

Stotter (1966) carried out experimental investigations on heat transfer for various methods of piston cooling at English Electric Co. Ltd., England, which were applied in calculations and predictions of piston temperatures [25]. It was shown that favourable cooling effect can be obtained by the oil leakages from the connecting rod small end. Flynn (1945) et. al found oil cooling as one of the efficient means for piston temperature control [26].

Otto Kruggel (1971) measured piston temperatures in an air cooled two-stroke gasoline engine [27]. The temperature measurements were carried out on the crown, in the ring zone, and at the cylinder with the objective to determine temperature fields of air cooled two stroke gasoline engines and validation of the computational model for pistons with flat crown of constant thickness at rational symmetrical heat flow.

Gerhard Woschni et. al found out the local heat transfer coefficients in the piston of a high speed diesel engine from experimentally measured piston temperature distribution [28]. Under different operating conditions of a high speed diesel engine the steady state temperature fields in the piston were measured and evaluated using relaxation method. With the help of these temperatures, the local heat transfer coefficients at the contour of the piston were determined. More than 60 temperature distributions in a piston of a high speed diesel engine were determined from measured temperatures at 20 discrete points of the piston for varied engine operating and cooling conditions. The heat flux through the piston and the heat transfer coefficients at the boundaries were also evaluated. The heat flow from the working fluid to the piston for different engine operating conditions were determined by a combination of cycle simulation and the electrolytic tank analogue. The heat transfer coefficeints determined at the cooled side of the piston were important to predict the thermal loading of engine componenets. Heubotter (1925) et. al analyzed the flow of heat in pistons [29]. Janeway carried out quantitative analysis of heat transfer in engines [30]. Paschkis et. al used electrical analogy method for determining unsteady state heat transfer through the piston [31].

Eugene J. Manganiello experimentally found out the piston temperatures in an air cooled engine for various operating conditions [3]. Indicated mean effective pressure, engine speed, fuel-air ratio, spark timing, cylinder temperature,

oil temperature, and oil vicosity were each seperately varied, the other conditions being held constant. The tests showed that the piston temperature increased with indicated horsepower, the variation being slightly greater for a change in indicated horsepower obtained by varying the indicated mean effective pressure than that obtained by increasing the speed. The piston temperatures varied linearily with cylinder temperature, increasing about 0.66^0 F per degree Fahrenheit rise in wall temperature; increasing rapidly with increased spark advance; and increased as the mixture was enriched to a relative fuel-air ratio of 0.77, decreasing with further enriching. Decreased oil viscosity resulted in a slight decrease of piston temperatures. Piston temperatures slightly decreased with an initial increase in oil out temperature and started increasing with a continued rise in oil temperature. A rough test indicated that the crankcase air and the oil thrown off from the bearings provide a small amount of piston cooling. National Advisory Committee for Aeronautics (NACA), successfully investigated the heat transfer process in air cooled engines and determined the amount of finning required for optimum cylinder cooling. As part of the program for study of piston cooling, NACA developed a satisfactory method of measuring piston temperatures at high engine speeds. A rough check of the piston cooling affected by the crankcase air and oil was also made [3]. Willis (1944) et. al found out the operating temeperatures and stresses in aluminum aircraft engine parts [32].

Sanders et. al analyzed the variation of piston temperature with piston dimensions and undercrown cooling [33]. They analyzed the operating temperatures at various points in the piston body on the basis of the experimentally determined surface heat transfer coefficients and boundary region temperatures, as well as arbitrarily selected surface coefficients. Surface heat transfer coefficients were estimated from the internal temeperature gradients obtained by hardness surveys of

aluminum pistons that had been operated under severe conditions in a liquid cooled, single cylinder test engine. Baker (1932) et. al analyzed the piston temperatures and their relation to piston design [34].

Wang et. al developed a simplified annular heat-pipe cooled piston crown (AHPCC) [35]. The annular heat pipe is an extension of reciprocating heat pipe. Due to its cylindrical shape, the heat pipe can comply with the piston structure and the engine operating environment. The annular heat pipe has the potential to cool the piston ring area effectively and thus maintain the piston rings at a reasonably uniform temeperature. Experimental investigations were conducted to verify the working mechamisms of the annular heat pipe under a reciprocating motion.

Varghese et. al used Steven and Webb correlation to find the local heat transfer coefficient at the underside of the piston cooled by oil jet [36].A numerical simulator was developed to give temeperature distributions within the piston for different engine operating conditions.

Chapter 3

Computational Model Development

In order to understand the oil jet cooling of automotive piston, a computational model needs to be developed. For this, general heat transfer equation in cylindrical coordinates with appropriate boundary conditions need to be solved. A weak formulation of the governing differential equation need to be developed for given geometry. The geometry of the surface in question is converted to grid for finite element analysis. Thereafter Steven and Webb correlation is applied to this grid in order to find out the heat transfer coefficient at the jet cooled surface. A code is developed using weak formulation and isotherms are drawn on the surface of piston. The effect of various operating parameters on piston cooling is investigated in detail.

3.1 Numerical Modeling

The governing differential equation for the piston in cylindrical coordinates is given by equation 3.1 [37].

$$\frac{\partial^2 T}{\partial r^2} + \frac{1}{r}\frac{\partial T}{\partial r} + \frac{\partial^2 T}{\partial z^2} = 0 \tag{3.1}$$

Knowing the boundary conditions, equation (3.1) can be solved by numerical methods. The necessary boundary conditions are the temperature and heat transfer coefficient of the medium in contact with the piston surfaces. There are four boundary conditions for cooling of piston:

1. The top crown in contact with the hot combustion gases, ie:-

$$+k\frac{\partial T}{\partial z} = q" \tag{3.2}$$

2. The sliding lubricated surface is in contact with the liner and the rings, ie:-

$$-k\frac{\partial T}{\partial r} = U(T - T_{coolant}) \tag{3.3}$$

3. The inside of the piston exposed either to the crankcase atmosphere or to a cooling oil, ie:-

$$+k\frac{\partial T}{\partial z} = h(T - T_{surrounding}) \tag{3.4}$$

If oil jet cooling is being used then $T_{surrounding} = T_{oiljet}$. In the absence of oil jet cooling $T_{surrounding} = T_{crankcase}$. In case of oil jet cooling h is convective heat transfer coefficient between piston surface and cooling oil jet. In absence of oil jet cooling h represents the convective heat transfer coefficient between piston surface and air in the crankcase.

4. From the physical and geometrical conditions only half portion of the piston can be taken for analysis, ie:- we can assume insulated conditions for the straight edge of the half cut piston.

$$\frac{\partial T}{\partial r} = 0 \tag{3.5}$$

The positive sign on the L.H.S. of equations (3.2) and (3.4) are because temperatures will be increasing with increasing z on the disk. 'k' (W/mK) is the thermal conductivity of the piston, which is normally made of aluminum. The local jet heat transfer coefficient was calculated from the corelations given by Stevens and Webb (1991) for axisymmetric, single-phase free round liquid jets impinging normally against a flat uniform heat flux surface [17]. The correlation for local heat transfer coefficient at the underside of the piston surface, h = f(r), is given by equtions (3.6) - (3.8).

$$\frac{Nu}{Nu_0} = (1 + f(r/d)^{-9})^{-1/9} \tag{3.6}$$

where

$$f(r/d) = ae^{b(r/d)} \tag{3.7}$$

The values of a and b in equation (3.7) are given in table 3.1. These values are found out by Steven and Webb experimentally.

d(mm)	2.2	2.3	4.1	5.8	8.9
a	1.13	1.141	1.34	1.48	1.57
b	-0.23	-0.2395	-0.41	-0.56	-0.7

Table 3.1: Values of a and b used in equation (3.7) [17]

Stagnation point Nusselt number for equation 3.6 is given by the following equation. Equation (3.8) is valid for Re = 4000 - 52000.

$$Nu_0 = 2.67Re^{0.567}Pr^{0.4}(z_0/d)^{-0.0336}(v/d)^{-0.237} \tag{3.8}$$

Simplified figure of oil jet cooling of piston is shown in figure 3.1. For the ease of explanation piston is assumed as a circular disk. The oil jet is situated at a distance z_0 vertically below the piston as shown in figure 3.1. In other words, the jet is axisymmetric. The upper surface of the piston corresponds to the combustion chamber side and is subjected to an average heat flux of $q^{"}$ (W/m^2), the averaging being carried out over a cycle. Heat is transferred from the periphery of the piston to the coolant water via piston rings and cylinder wall. A typical coolant water temperature is 72^0 C [38]. An estimated overall heat transfer coefficient U (W/m^2K) was used. The bottom of the piston is hit by the oil jet. The piston moves inside the cylinder with a variable velocity, which is a function of crank angle, rotational speed, length of the crank and the connecting rod. For the ease of simulation, the piston is assumed to be stationary and the undercrown surface is hit by the oil jet with a velocity which is the relative velocity, $v = v_{jet(absolute)}$ - v_{piston} averaged over one cycle. The piston and crankshaft mechanism is depicted in figure 3.2. The velocity of the piston, v_{piston}(m/s) is given by the equation 3.9 [39].

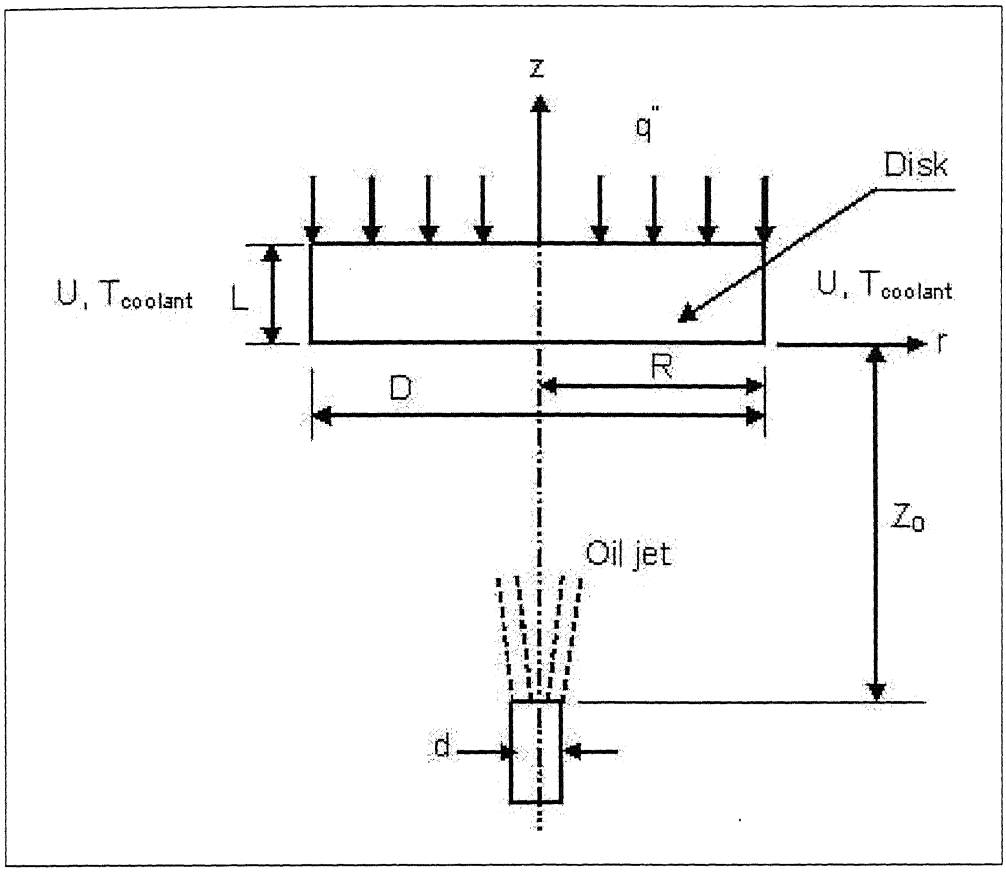

Figure 3.1: Coordinate System and Pictorial View of Notations Used for Oil Jet Cooling

$$v_{piston} = \frac{ds}{dt} = \omega R_c \sin\theta + \frac{\omega R_c^2 \sin\theta \cos\theta}{(L^2 - R_c^2 \sin^2\theta)^{1/2}} \tag{3.9}$$

where

θ = Crank angle in degrees = ωt, $0 \leq t \leq t_{cycle}$

R_c = Length of the crank, m (AB in figure 3.2)

L = Length of the connecting rod, m (BC in figure 3.2)

ω = Angular speed of the crank shaft = $2\pi N$radians/sec

N = Rotational speed of the engine, rpm

t = Time, s

t_{cycle} = Cycle time, s = $\frac{nN}{60}$where n = 2 for a four stroke engine

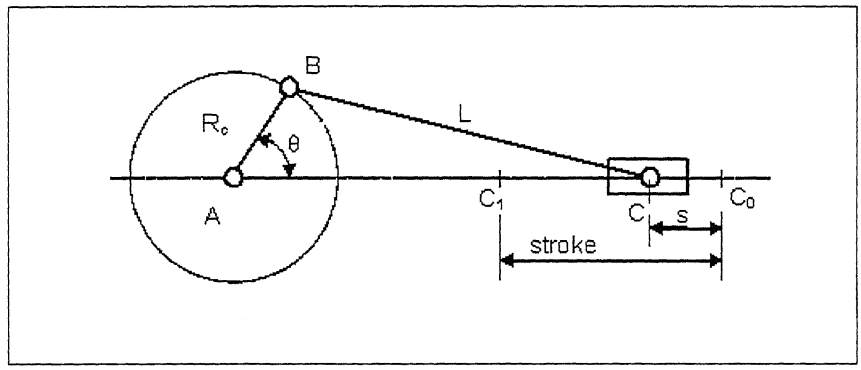

Figure 3.2: Crank and Connecting Rod Mechanism

3.2 Weak Formulation

The governing differential equation 3.1 is solved using Finite Element Analysis (FEA) methods. In the development of the weak form, we consider an arbitrarily typical element. It is assumed that Ω^e is such an element of the finite element mesh, which is quadrilateral. A finite element model of equation 3.1 over Ω^e is developed. The variational statement of the governing differential equation 3.1 is:

$$2\pi \int \int_{\Omega^e} w(\frac{1}{r}\frac{\partial}{\partial r}(k_r r\frac{\partial T}{\partial r}) + \frac{\partial}{\partial z}(k_z\frac{\partial T}{\partial z}))\ r\ dr\ dz \tag{3.10}$$

$$2\pi[\{\int\int_{\Omega^e} w\frac{\partial}{\partial r}(k_r r\frac{\partial T}{\partial r})\ dr\ dz\} + \{\int\int_{\Omega^e} wr\frac{\partial}{\partial z}(k_z\frac{\partial T}{\partial z})\ dr\ dz\}] = 0$$

$$2\pi[\int\int_{\Omega^e}\{(k_r r\frac{\partial T}{\partial r})\frac{\partial w}{\partial r} + k_z r\frac{\partial w}{\partial z}\frac{\partial T}{\partial z}\}\ dr\ dz - \oint_{\Gamma^e} r(wk_r\frac{\partial T}{\partial r}n_r + wk_z\frac{\partial T}{\partial z}n_z)\ ds] = 0$$

$$2\pi[\int\int_{\Omega^e}(k_r\frac{\partial T}{\partial r}\frac{\partial w}{\partial r} + k_z\frac{\partial w}{\partial z}\frac{\partial T}{\partial z})r\ dr\ dz - \oint_{\Gamma^e} wq_n r\ ds] = 0 \tag{3.11}$$

where

$$q_n = k\nabla T = k_r\frac{\partial T}{\partial r}n_r + k_z\frac{\partial T}{\partial z}n_z$$

Using Lagrange interpolation function

$$T = \sum_{j=1}^{n} T_j^e\psi_j^e(r,z) \tag{3.12}$$

The specific form of ψ_j^e is derived for linear rectangular elements [40]. Using the Rayleigh-Ritz method of approximation

$$w = \psi_i^e \tag{3.13}$$

the final form of the equation 3.10 in matrix form is

$$[K_{ij}^e + H_{ij}^e]\{T_j^e\} = \{Q_i^e\} + \{P_i^e\} \tag{3.14}$$

where

$$K_{ij}^e = 2\pi \int\int_{\Omega^e} (k_r \frac{\partial \psi_i^e}{\partial r} \frac{\partial \psi_j^e}{\partial r} + k_z \frac{\partial \psi_i^e}{\partial z} \frac{\partial \psi_j^e}{\partial z})\, r\, dr\, dz$$

$$H_{ij}^e = 2\pi \oint_{\Gamma^e} h^e \psi_i^e \psi_j^e\, r\, ds$$

$$Q_i^e = 2\pi \oint_{\Gamma^e} q_n \psi_i^e\, r\, ds$$

$$P_i^e = 2\pi \oint_{\Gamma^e} h^e T_\infty^e \psi_i^e\, r\, ds$$

It must be noted that it is not essential to calculate H_{ij}^e, Q_i^e and P_i^e when a portion of Γ^e does not coincide with the boundary Γ of the total domain Ω. For an interior element (ie., one that does not have any of its sides on the boundary of the problem) the contribution from the boundary integral cancels with the similar contributions from adjoining elements of the mesh.

3.3 Computer Implementation

Flow diagram for the numerical modeling work of oil jet cooling of pistons is shown in figure 3.3. The finite element program developed consists of three basic parts:

1. Preprocessor
2. Processor
3. Postprocessor

In the preprocessor part of the program, the input data of the problem are given. This input data includes the geometry of the piston, number of meshes in r and z direction, conductivity of the piston material, heat transfer coefficients

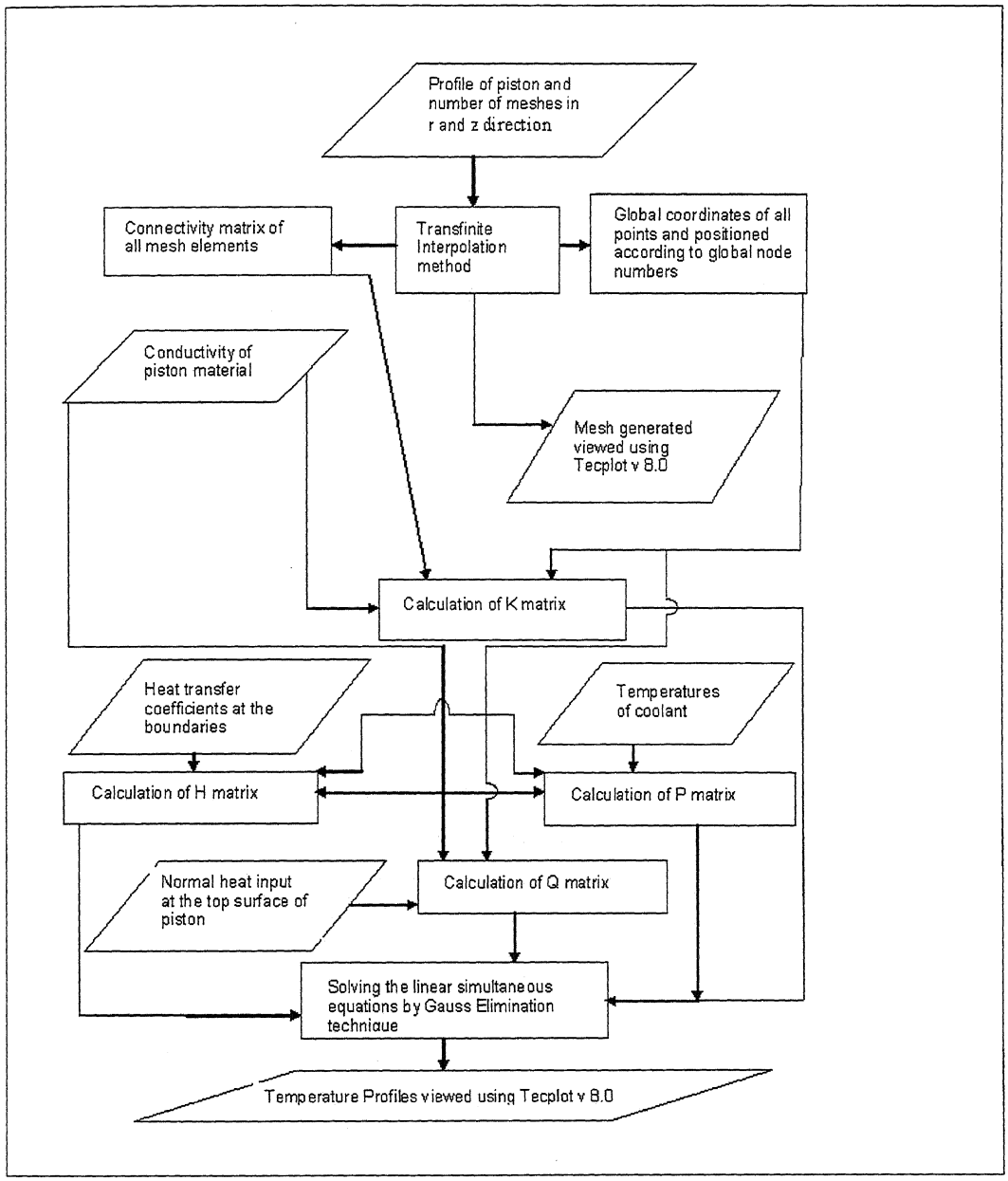

Figure 3.3: Flow Diagram of Numerical Work

at the boundaries, temperatures of the coolants and the normal heat input at the top surface of the piston.

In the processor part, all steps in the finite element method, except for postprocessing are performed. First the profile of the piston is divided into quadrilateral elements using Transfinite Interpolation technique. Transfinite Interpolation method is explained in detail in appendix A. Further steps include generation of the element matrices using numerical integration, global coordinates of all points, connectivity matrix of all mesh elements. For numerical integration, Gauss-Legendre Quadrature two-point formula was used. Readers are requested to refer [41] for further information. Solution of the linear simultaneous equations was obtained by Gauss Elimination technique. For further refinement of the solution obtained by Gauss Elimination technique, Gauss-Siedel Iterative technique was used.

In the postprocessor part, output data are processed in a desired format for plotting isotherms. For plotting the structured grid as well as isotherms, Tecplot v 8.0 software was used. For plotting the other graphs Matlab v 6.5 software was used.

Detailed steps of running the computer code, that was developed for the current investigation, are given in appendix B.

Chapter 4

Experimental Setup

4.1 Objective of the Experimental Setup

The objective of setting up an experiment was to validate the computational model for oil jet cooling of flat plate experimentally. The second objective was to investigate the conditions, under which the oil jet cooling of the flat plate/piston start contributing significantly towards the non-tail pipe emissions through mist and smoke by oil jet breakup and localised boiling.

4.2 Schematic of Experimental Setup

Schematic of the experimental setup is shown in figure 4.1. Further details and specifications of subparts of the experimental setup are explained in detail in the following section.

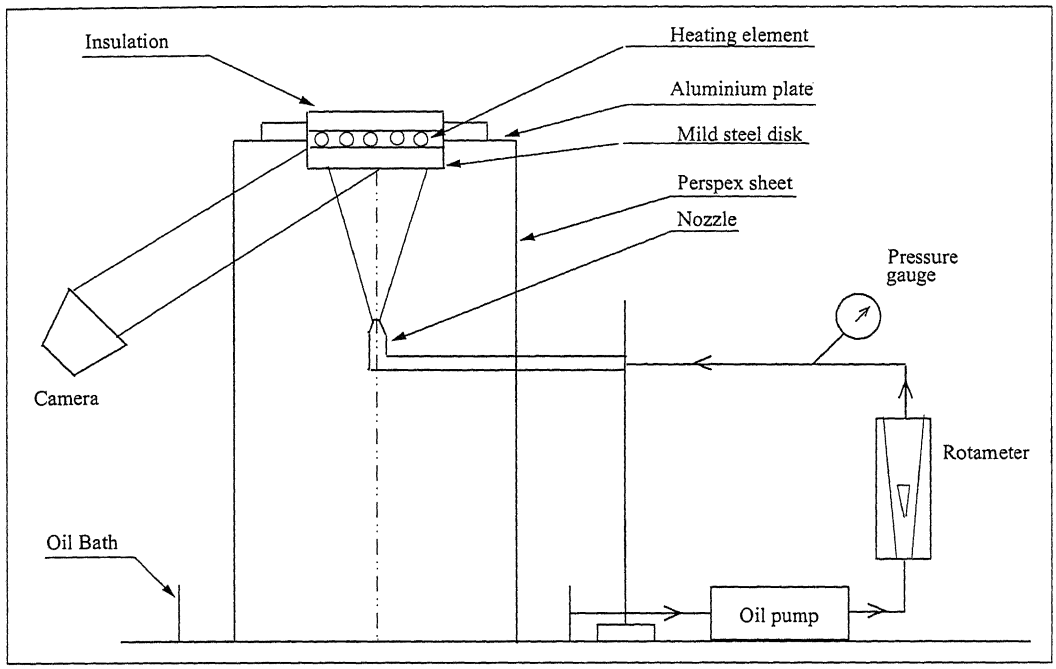

Figure 4.1: Schematic of Experimental Setup

4.3 Description of Experimental Setup

Photograph of the experimental set up installed in the energy conversion laboratory of mechanical engineering department is shown in figure 4.2. Experimental set up consists of a square cross-sectional perspex enclosure of width 270 mm and height 600 mm. On the left hand side of the enclosure there is a slot of 16 mm width to make way for the nozzle (for vertical movement) with its holder. Figure 4.3 shows the top view of the perspex enclosure. The perspex enclosure was fabricated using 2 perspex sheets of 290 mm width and 600 mm length, 1 perspex sheet of 270 mm width and 600 mm length and 2 perspex sheets of 127 mm width and 600 mm length. To make the enclosure, two perspex sheets were taken at a time, held at 90^0 with the edge of one perspex sheet over the face of other perspex sheet. Then chloroform was injected and perspex sheets were rubbed against

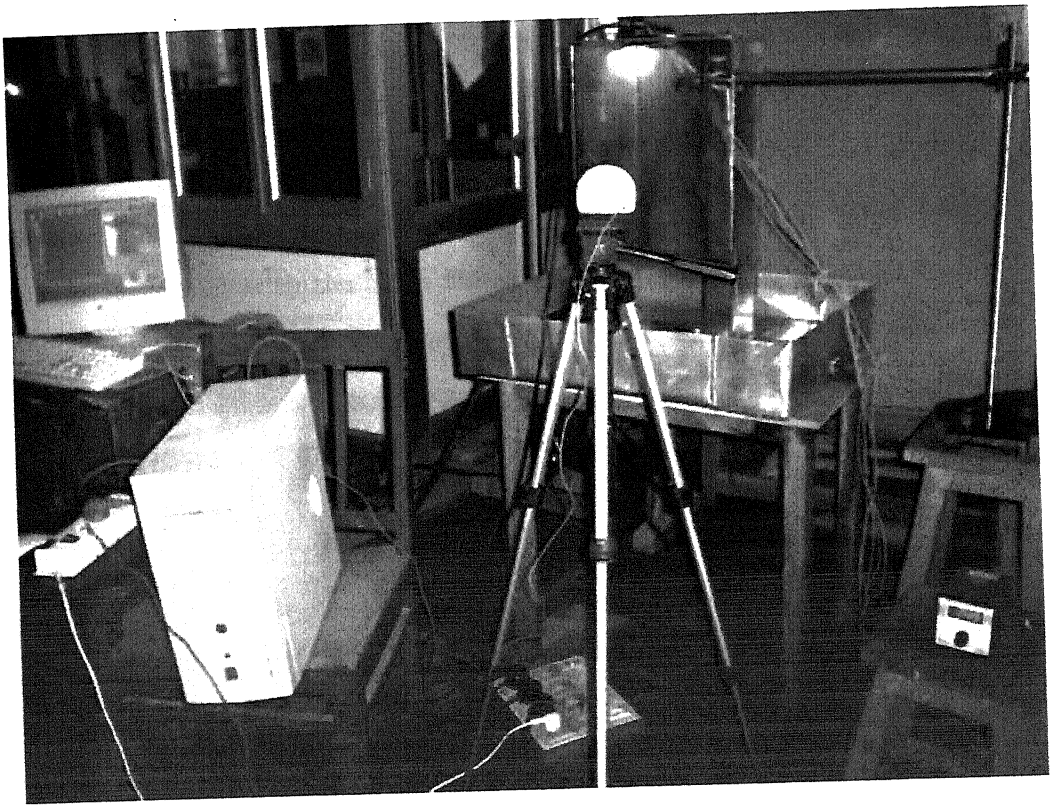

Figure 4.2: Experimental Set Up

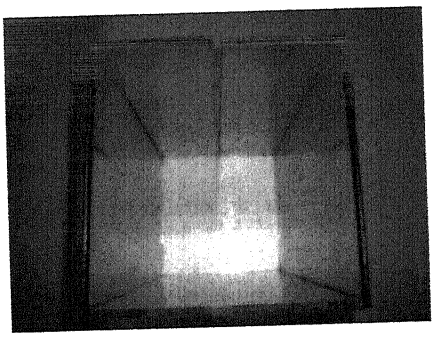

Figure 4.3: Top View of Perspex Enclosure

each other. Chloroform acts as adhesive and the sheet join together. After completing the fabrication, perspex enclosure was kept in an aluminum tank so that it can collect the free falling oil jet and droplets, which fall down after hitting the flat

plate/piston. Width of the aluminum tank is 700 mm and length 870 mm. Capacity of the aluminum tank is 60 litres. Aluminum tank was fabricated from aluminum sheet by thermit welding process. Within the aluminum tank, two circular disks of diameter 90 mm and height 65 mm were kept so that the perspex enclosure does not come in contact with the oil in the tank. The circular disks had a slot of 12 mm width and 10 mm depth to accommodate the faces of the enclosure. Aluminum tank with perspex enclosure is shown in figure 4.4. The top surface of the perspex

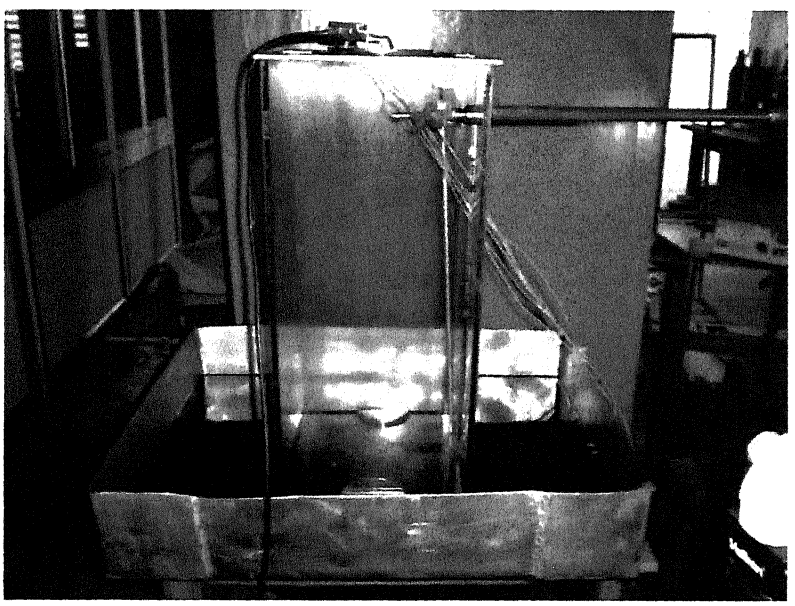

Figure 4.4: Aluminum Tank with Perspex Enclosure

enclosure was covered with an aluminum plate of width 310 mm and length 310 mm. The thickness of the aluminum plate is 6 mm. A disk of 210 mm is removed from the aluminum plate to make provision for a flat plate. Aluminum plate with the flat plate is shown in figure 4.5.

The oil in the tank has to be raised to a maximum height of 550 mm. For this we need an oil pump. Assuming the losses in the pipeline to be 10 mm, which actually could be lower. Further it is required that the maximum velocity of

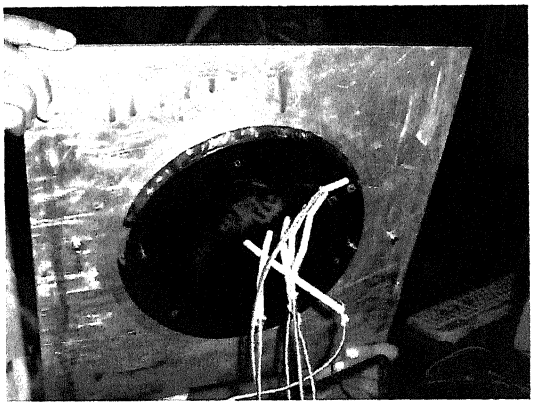

Figure 4.5: Aluminum Top Plate and Flat Plate

the jet at the nozzle end should be 50 m/s.

$$\begin{aligned}
\text{Work head required in m} &= 560 \text{ x } 10^{-3} + \frac{50^2}{2 \text{ X } 9.81} \\
&\simeq 128 \text{ m} \\
\text{Working Pressure (P)} &= \rho_{oil} g h \\
&= 900 \text{ x } 9.81 \text{ x } 128 \\
&= 11.3 \text{ bar}
\end{aligned}$$

Assuming the diameter of the nozzle (d) to be 3 mm,

$$\begin{aligned}
\text{Flow rate of oil (Q)} &= \tfrac{\pi}{4} d^2 \text{ x } 50 \\
&= 3.53 \text{ x } 10^{-4}\ m^3/s \\
&= 0.353 \text{ litres/s } = 21.18 lpm \\
\text{Power input to the pump required} &= \text{P x Q} \\
&= 11.3 \text{ x } 10^5 \text{ x } 3.53 \text{ x } 10^{-4} \\
&\simeq 400\ W
\end{aligned}$$

As it is clear from the above calculations, we need a pump of 0.5 horsepower rating. A motor of 0.5 hp rating, shaft speed of 1225 rpm (Crompton Greaves make) was

selected. A pump of rated capacity 20 litres per minute, shaft speed of 1225 rpm was selected. The motor was coupled to the pump with the help of a bush coupling. Motor and pump with bush coupling are shown in figure 4.6. The motor and pump

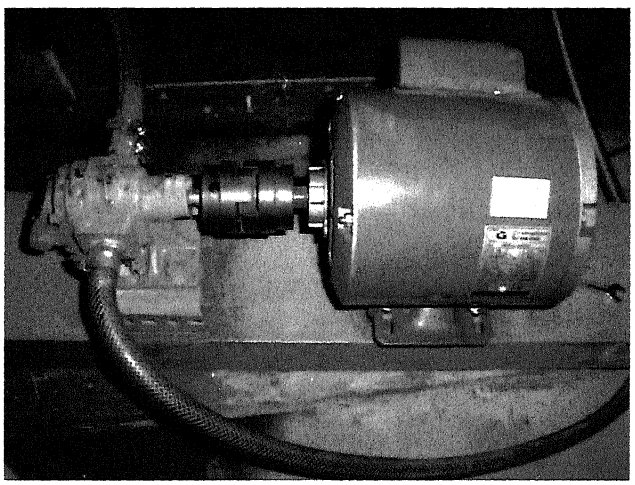

Figure 4.6: Motor and Pump

assembly was mounted on a C channel and the C channel was mounted on a wooden board in order to dampen out the vibrations. The hose connecting the output of the pump to the nozzle was a hose, which is able to withstand high temperatures. The hose has three layers. The innermost layer is made of rubber. On the top of it there is a layer of flexible steel rods. The uppermost layer is again of rubber. This types of hose are normally used to carry oil and high temperature applications like fire brigade. A throttle valve is used to control the flow pressure and thus velocity of the jet. A rotameter is connected in the line to measure the oil flow rate. Rotameter is capable of measuring a flow rate of 3 - 30 litres per minute. The make of the rotameter is Mahavir and is capable to withstand high temperatures. Rotameter is shown in figure 4.7. Pressure gauge was also connected to measure the oil pressure. The range of the oil pressure gauge is from 0 to 15 bar. The make of the pressure gauge is Karnataka Instruments. Pressure gauge is shown in figure 4.8.

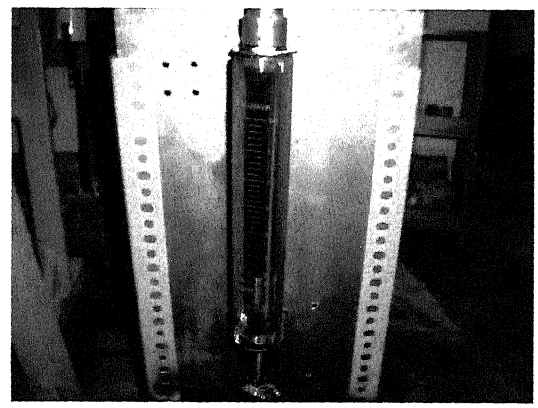

Figure 4.7: Rotameter

Figure 4.8: Pressure Gauge

Experimental validation of the numerical simulator was carried out on a flat plate of diameter 190 mm and 4 mm thickness. On the top of the flat plate, there is a spiral heating coil of rating 1200 watts. At the time of conducting the experiments, the top surface of the heater was covered with an absetos sheet to prevent the loss of heat. The flat plate with heater arrangement is shown in figure 4.9. The flat plate is divided into six equispaced points from the center, where six K-type thermocouples are riveted, marked as 'x' in figure 4.10.

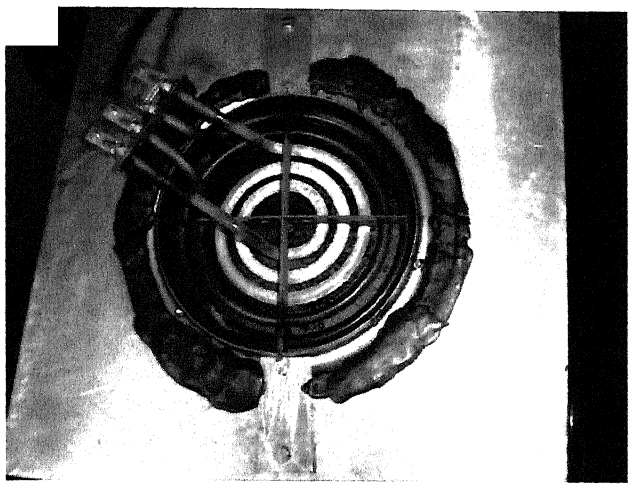

Figure 4.9: Flat Plate with Heater

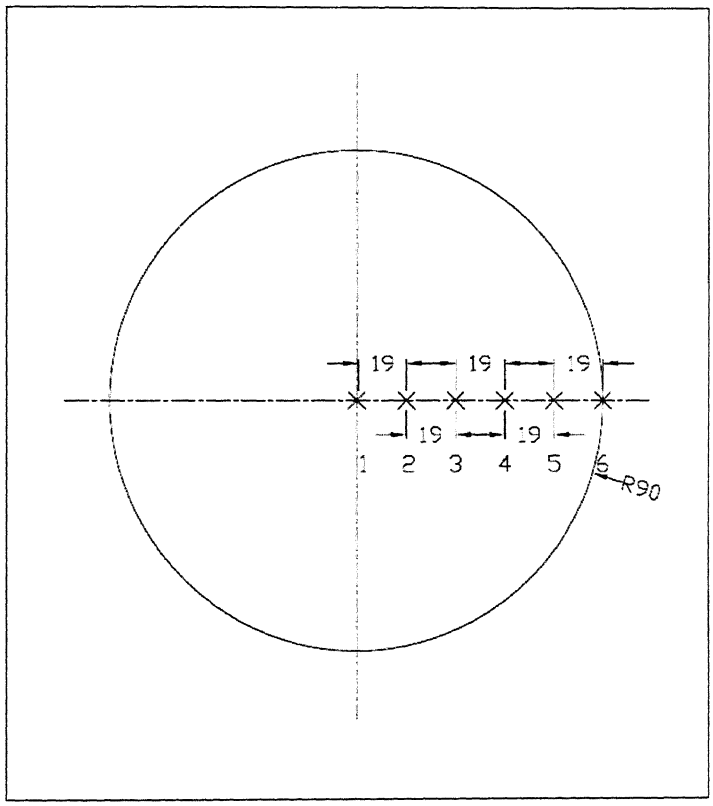

Figure 4.10: Position of Points on the Flat Plate.

The temperatures obtained by thermocouples are recorded on a six point digital temperature indicator. The least count of the six point digital temperature indicator is 1^0C. The temperature indicator was of make Pedigree and the model number was DTI4006. The temperature range of the indicator was from 0 ^{0}C to 999 ^{0}C. The temperature indicator is shown in figure 4.11.

Figure 4.11: 6 Point Digital Temperature Indicator

Oil used for carrying out the experiments was SAE 40 oil. The nozzle used for study was a production grade nozzle of Cummins engine, having a diameter of 3 mm as shown in figure 4.12. For mist generation studies Kensington web camera

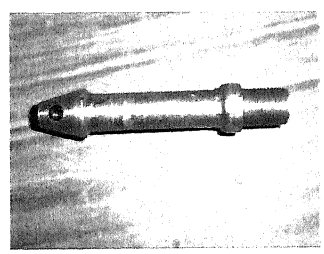

Figure 4.12: Nozzle

was used for shooting the mist generated, when high velocity jet hits the hot plate. Frame speed of the web camera is 15 fps. The web camera is shown in figure 4.13.

Mahindra and Mahindra MDI 2500 diesel engine piston was used for conducting the numerical investigations. Dimensions of MDI 2500 piston are shown in figure 4.14.

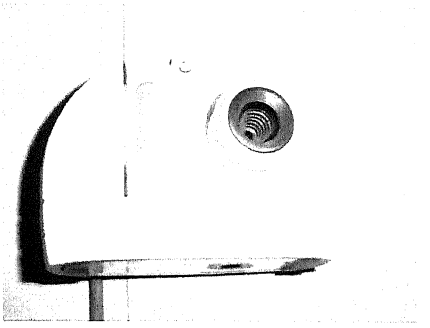

Figure 4.13: Web Camera

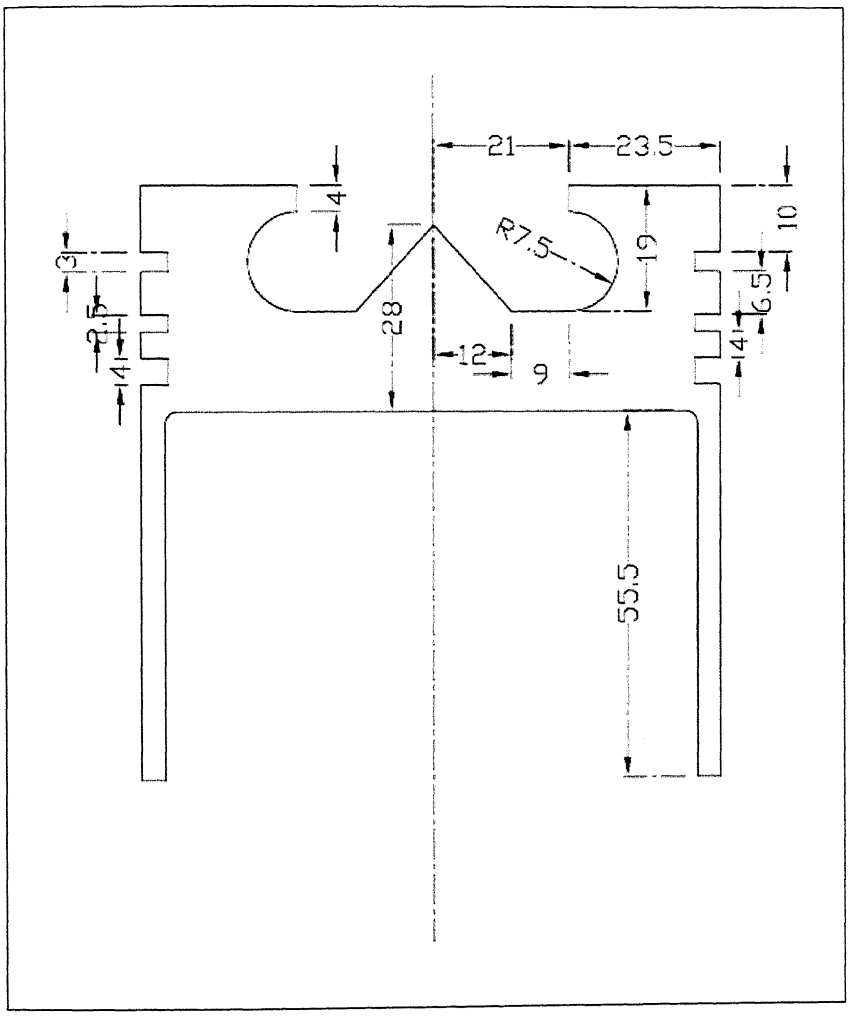

Figure 4.14: Dimensions of MDI 2500 Piston

Chapter 5

Results And Discussions

This study is divided in two main part.

1. Computational investigation of the hot plate and experimental validation of oil jet cooling for verification of the computer model.

2. Application of this validated model to a piston of production grade and prediction of temperatures at various locations followed by evaluation of the effect of oil jet cooling.

5.1 Computational and Experimental Investigation of Flat Plate Cooling

Experimental validation of the numerical simulator was carried out on a flat plate of diameter 190 mm and 4 mm thickness. On the top of the flat plate there is a heating coil of rating 1200 watts (which is equivalent to heat input of 42.3 kW/m^2). The flat plate was cooled from the underside by a production grade oil cooling nozzle supplied by Cummins engines. The diameter of the nozzle hole

is 3 mm. Impingement vertical distance as well as the velocity of the jet are the variable parameters used to validate the numerical simulator. From the center of the flat plate, 6 equi-spaced points are connected to 6 K-type thermocouples. The temperatures obtained by the thermocouples were measured using a six point digital temperature indicator. The least count of the digital temperature indicator is 1 ^{0}C. In the following pages, the temperatures predicted at the six points with the help of numerical simulator as well as those obtained experimentally are shown graphically. The percentage difference between the numerical value and the experimental value are shown in tabular form.

5.1.1 Experimental Validation of Model for Flat Plate by changing the Nozzle Location

The nozzle location was varied and validation of the model for flat plate was carried out for various nozzle locations.

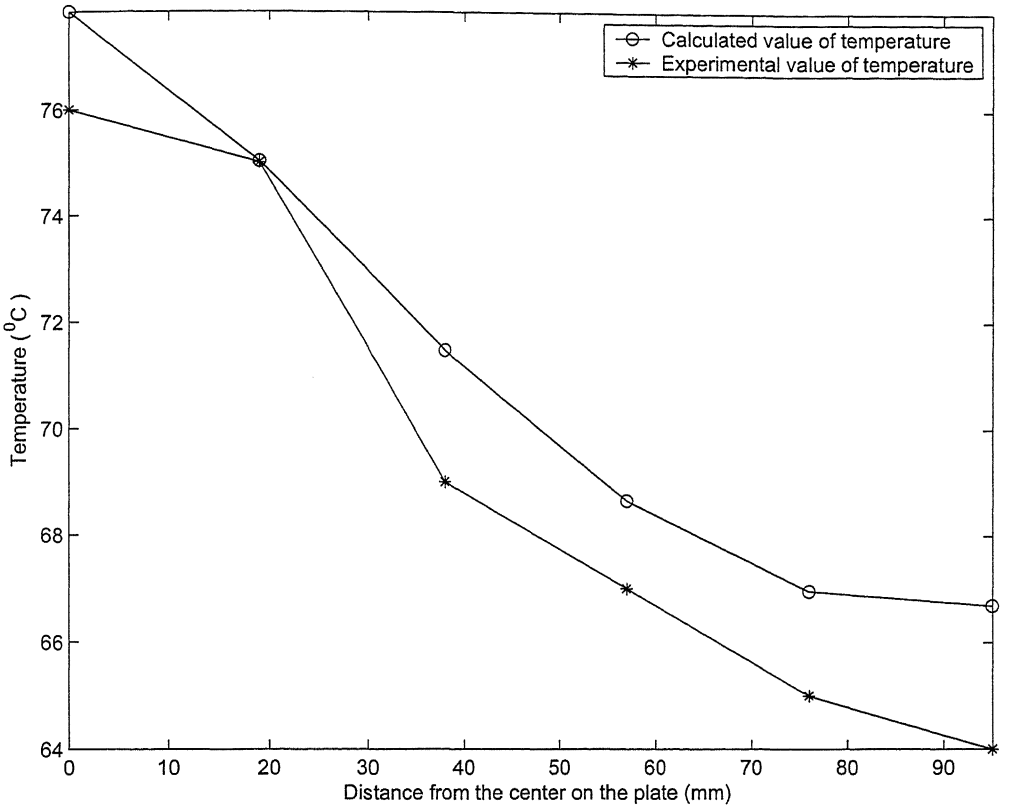

Figure 5.1: Temperatures Predicted Numerically and Experimentally for an Oil Cooled Flat Plate Configuration for z = 85 mm

Distance from plate center	Calculated value of temperature	Experimental value of temperature	% difference
0	77.8	76	2.44
19	75.0	75	0.033
38	71.4	69	3.58
57	68.6	67	2.47
76	66.9	65	3
95	66.6	64	4.2

Table 5.1: Percentage Difference Between Numerical and Experimental Values of Temperatures in an Oil Jet Cooled Flat Plate for z = 85 mm

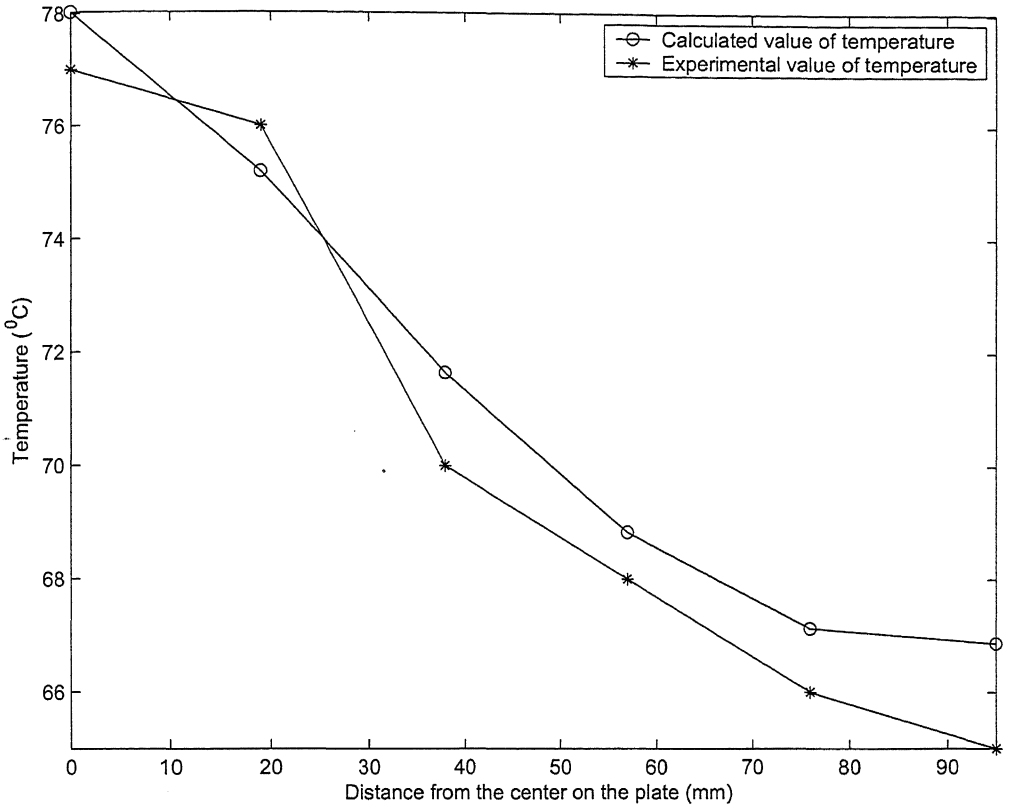

Figure 5.2: Temperatures Predicted Numerically and Experimentally for an Oil Cooled Flat Plate Configuration for z = 105 mm

Distance from plate center	Calculated value of temperature	Experimental value of temperature	% difference
0	78.0	77	1.33
19	75.1	76	- 1.072
38	71.6	70	2.33
57	68.8	68	1.22
76	67.1	66	1.71
95	66.8	65	2.87

Table 5.2: Percentage Difference Between Numerical and Experimental Values of Temperatures in an Oil Jet Cooled Flat Plate for z = 105 mm

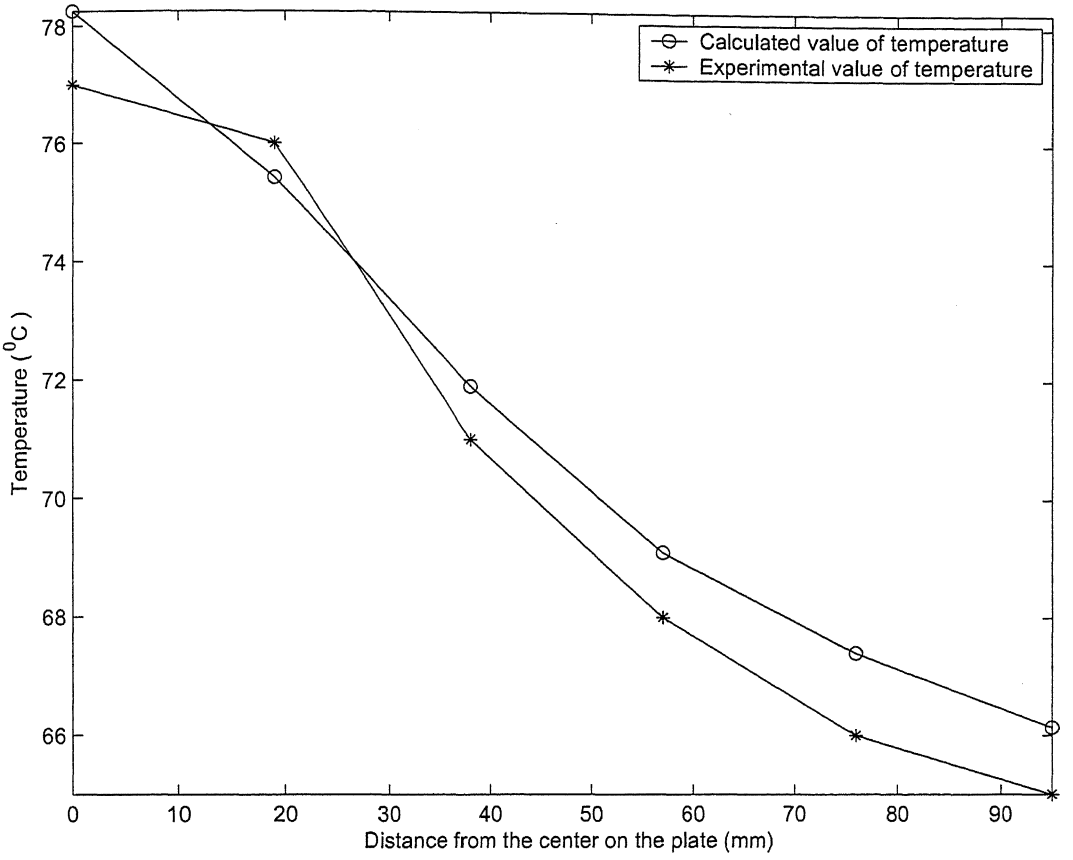

Figure 5.3: Temperatures Predicted Numerically and Experimentally for an Oil Cooled Flat Plate Configuration for z = 125 mm

Distance from plate center	Calculated value of temperature	Experimental value of temperature	% difference
0	78.2	77	1.63
19	75.4	76	- 0.77
38	71.8	71	1.26
57	69.0	68	1.62
76	67.3	66	2.11
95	66.1	65	2.14

Table 5.3: Percentage Difference Between Numerical and Experimental Values of Temperatures in an Oil Jet Cooled Flat Plate for z = 125 mm

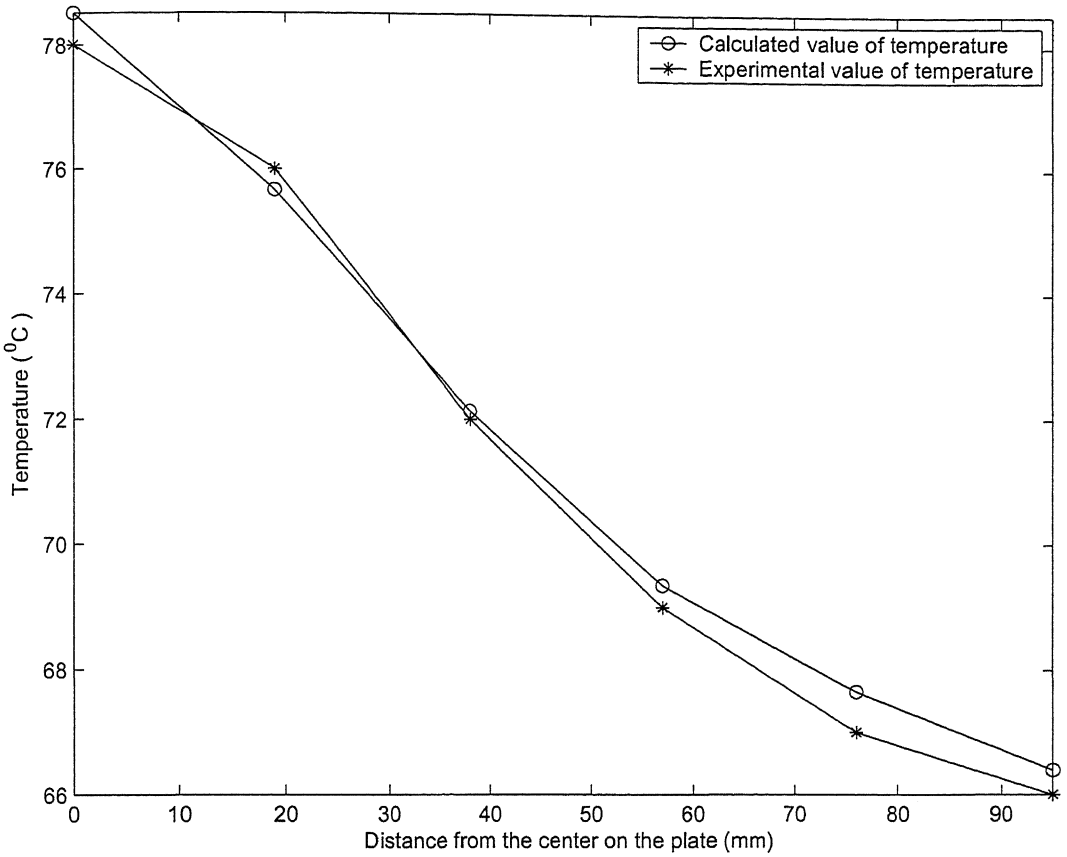

Figure 5.4: Temperatures Predicted Numerically and Experimentally for an Oil Cooled Flat Plate Configuration for z = 145 mm

Distance from plate center	Calculated value of temperature	Experimental value of temperature	% difference
0	78.5	78	0.66
19	75.6	76	- 0.44
38	72.1	72	0.18
57	69.3	69	0.51
76	67.6	67	0.97
95	66.3	66	2.11

Table 5.4: Percentage Difference Between Numerical and Experimental Values of Temperatures in an Oil Jet Cooled Flat Plate for z = 145 mm

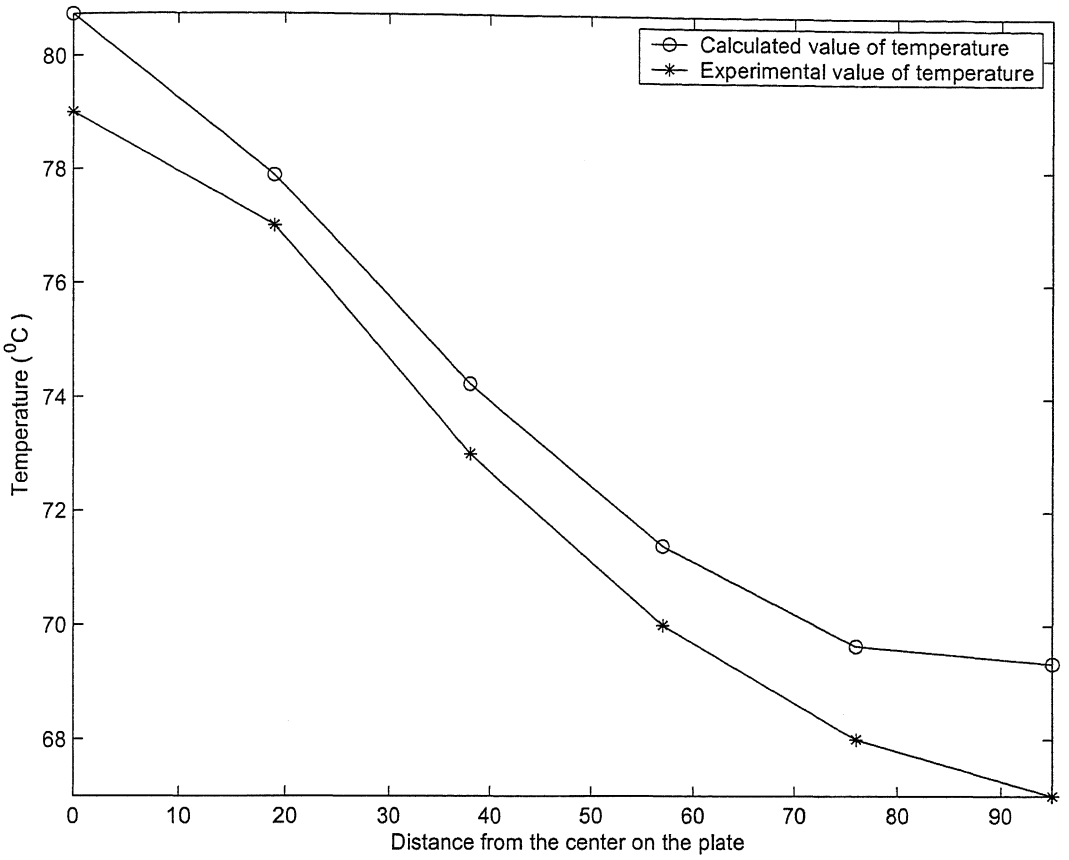

Figure 5.5: Temperatures Predicted Numerically and Experimentally for an Oil Cooled Flat Plate Configuration for z = 165 mm

Distance from plate center	Calculated value of temperature	Experimental value of temperature	% difference
0	80.7	79	2.2
19	77.8	77	1.1
38	74.2	73	1.69
57	71.3	70	1.98
76	69.6	68	2.41
95	69.3	67	3.48

Table 5.5: Percentage Difference Between Numerical and Experimental Values of Temperatures in an Oil Jet Cooled Flat Plate for z = 165 mm

5.1.2 Experimental Validation of Model for Flat Plate by changing the Oil Jet Velocity

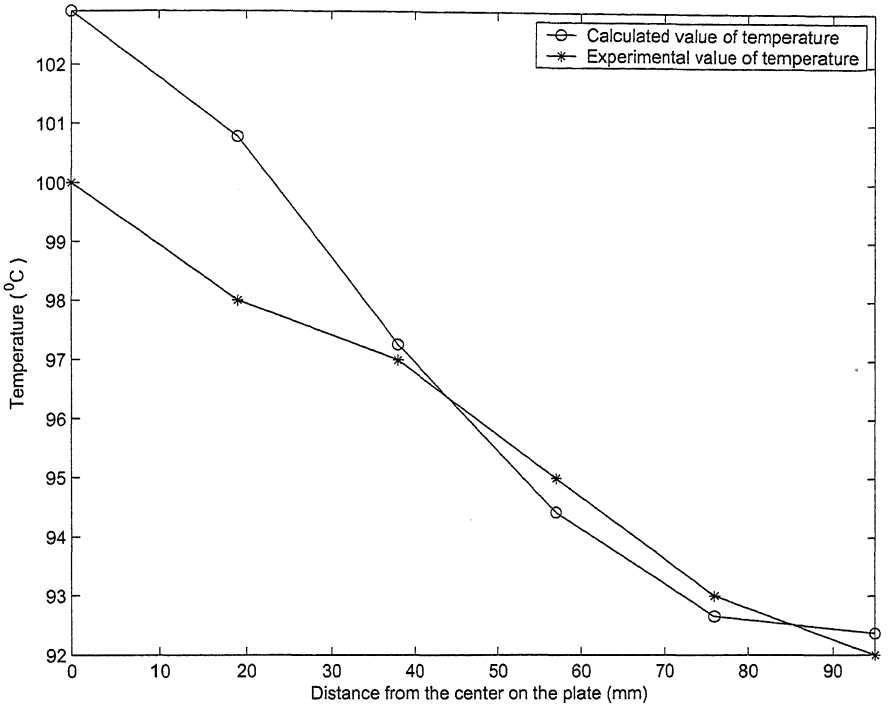

Figure 5.6: Temperatures Predicted Numerically and Experimentally for an Oil Cooled Flat Plate Configuration for v = 30 m/s

Distance from plate center	Calculated value of temperature	Experimental value of temperature	% difference
0	102.9	100	2.91
19	100.7	98	2.83
38	97.2	97	0.27
.57	94.4	95	- 0.61
76	92.6	93	- 0.37
95	92.3	92	0.39

Table 5.6: Percentage Difference Between Numerical and Experimental Values of Temperatures in an Oil Jet Cooled Flat Plate for v = 30 m/s

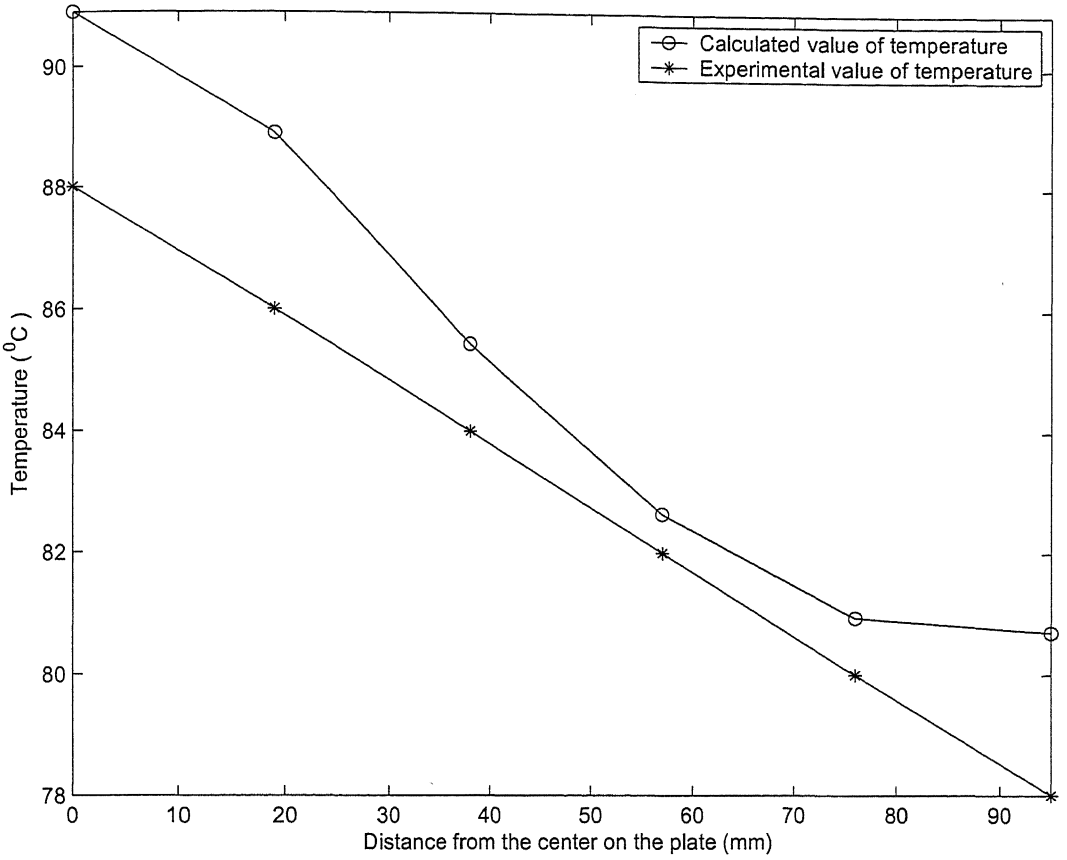

Figure 5.7: Temperatures Predicted Numerically and Experimentally for an Oil Cooled Flat Plate Configuration for v = 40 m/s

Distance from plate center	Calculated value of temperature	Experimental value of temperature	% difference
0	90.9	88	3.3
19	88.8	86	3.36
38	85.4	84	1.71
57	82.6	82	0.77
76	80.9	80	1.17
95	80.7	78	3.46

Table 5.7: Percentage Difference Between Numerical and Experimental Values of Temperatures in an Oil Jet Cooled Flat Plate for v = 40 m/s

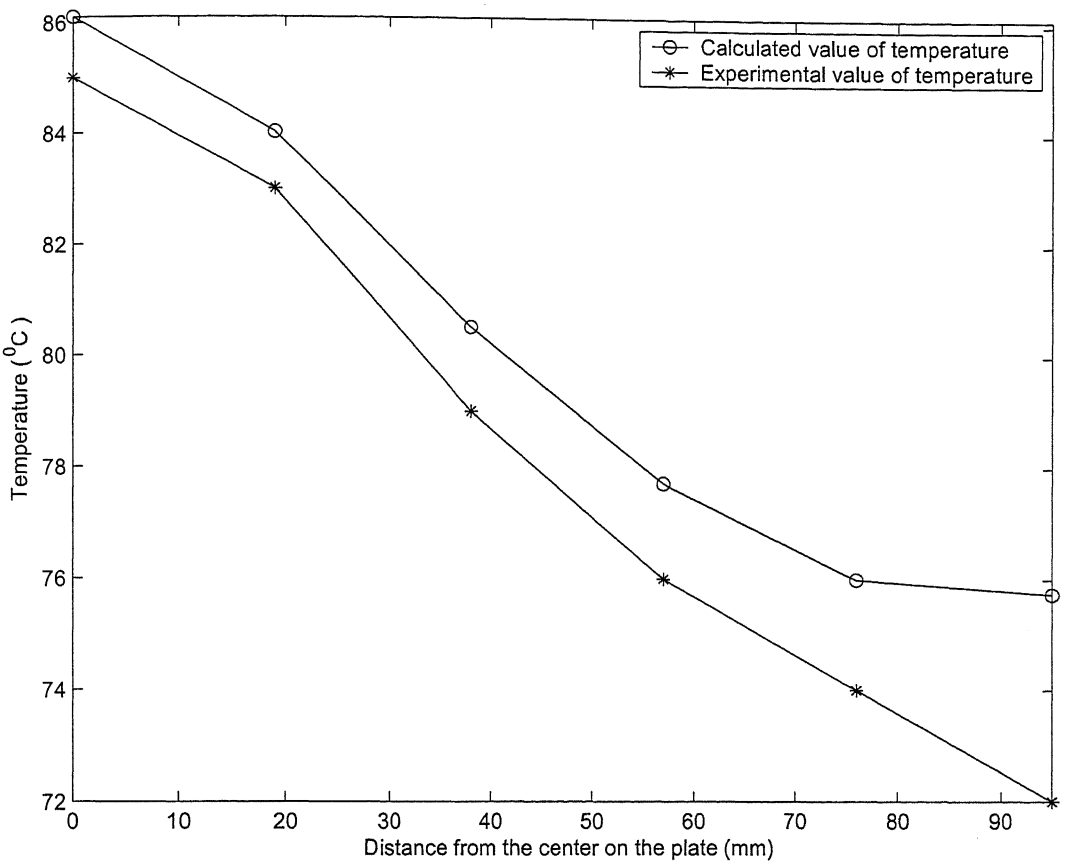

Figure 5.8: Temperatures Predicted Numerically and Experimentally for an Oil Cooled Flat Plate Configuration for v = 50 m/s

Distance from plate center	Calculated value of temperature	Experimental value of temperature	% difference
0	86.1	85	1.3
19	84.0	83	1.24
38	80.5	79	1.93
57	77.7	76	2.26
76	75.9	74	2.7
95	75.7	72	5.18

Table 5.8: Percentage Difference Between Numerical and Experimental Values of Temperatures in an Oil Jet Cooled Flat Plate for v = 50 m/s

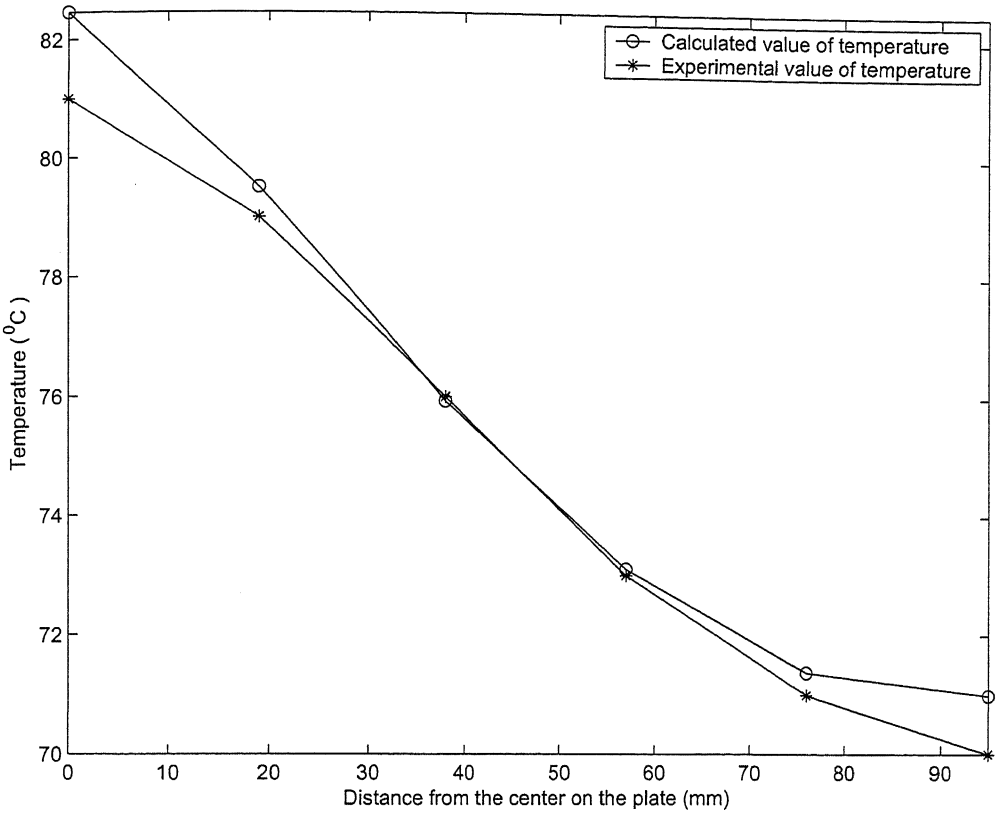

Figure 5.9: Temperatures Predicted Numerically and Experimentally for an Oil Cooled Flat Plate Configuration for v = 60 m/s

Distance from plate center	Calculated value of temperature	Experimental value of temperature	% difference
0	82.4	81	1.8
19	79.5	79	0.64
38	75.9	76	- 0.09
57	73.1	73	0.14
76	71.3	71	0.53
95	70.9	70	1.4

Table 5.9: Percentage Difference Between Numerical and Experimental Values of Temperatures in an Oil Jet Cooled Flat Plate for v = 60 m/s

Maximum percentage difference between numerical and experimental value is 5 % where as the minimum percentage difference between numerical and experimental value is 0.09 %. Most of the percentage differences were between 1 to 2 %. In most of the cases there were large differences between calculated value and experimental value for the right hand corner point. Probable reason could be that convective heat transfer coefficient on the air side is not exactly known. The average percentage difference between numerical and experimental value is 1.6 %.

5.2 Numerical Investigations of Oil Jet Cooling of Pistons

The piston used for numerical investigation is a production grade piston from Mahindra and Mahindra Direct Injection MDI 2500 diesel engine. The input parameters for the simulation are as follows:

Piston Diameter (D):	89 mm
Oil jet impingement distance from BDC (z):	55 mm
Diameter of jet (d):	2.3 mm
Oil temperature:	100 ^{0}C
Oil type:	SAE 15W40
Oil flow rate (Q):	8 x 10^{-5} m^3/s (4.8 litres/minute)
Specific heat (C_p):	2.219 kJ/kgK
Oil thermal conductivity (k):	0.137 W/mK
Density of oil (ρ):	847 kg/m^3
Kinematic viscosity of oil (ν):	14.1 x 10^{-6} m^2/s
Aluminum thermal conductivity (k):	137 W/mK
Jet velocity (v):	20 m/s

Table 5.10: Input Parameters for Numerical Simulation

Structured mesh was generated within the piston profile using Trans-finite Interpolation method. 770 quadrilateral elements were taken. Grid indepen-

dence test is shown in figure 5.10. For performing the grid independence test, a node which does not get affected with the increase in number of grids is selected. Number of grids are varied and variation of the parameter (here temperature) under study at the selected node is observed. The parameter under study at the selected node, either increases or decresaes significantly with the variation in the number of grids. After certain number of grids, the parameter under study at the selected node almost remains constant with the increase in the number of grids. The lowest number of grids after which the parameter remains constant is selected as the number of grids for further investigations. Mesh generated within the half axisymmetric

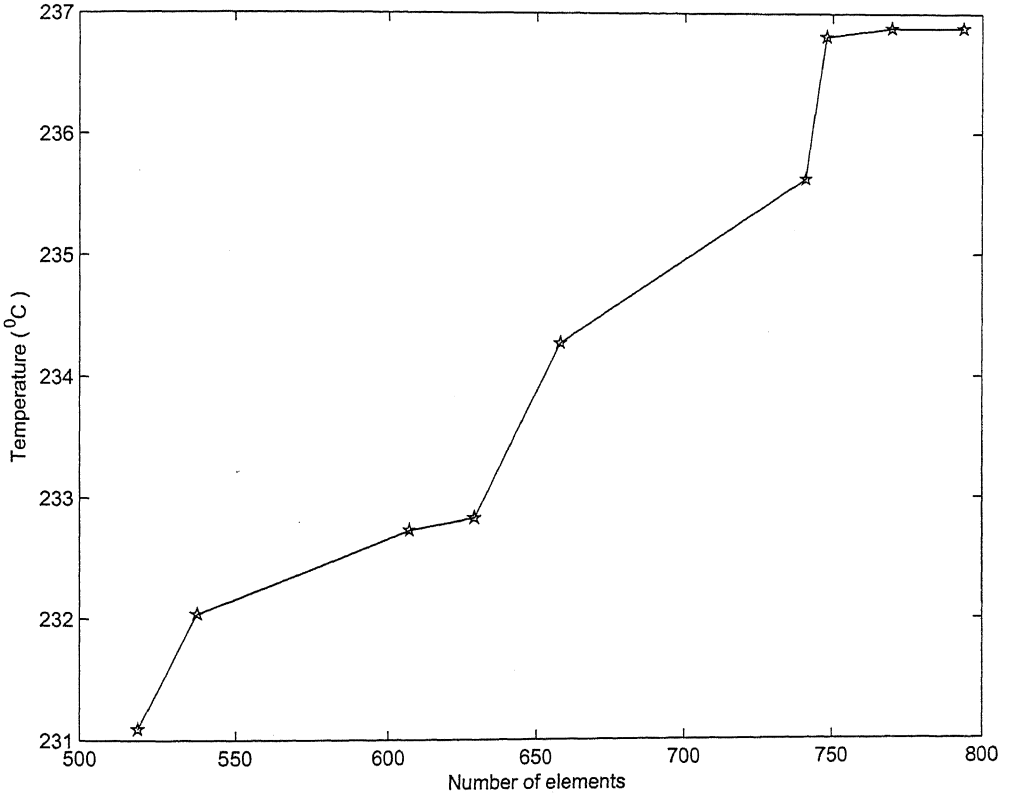

Figure 5.10: Grid Independence Test.

segment of the piston is shown in figure 5.11.

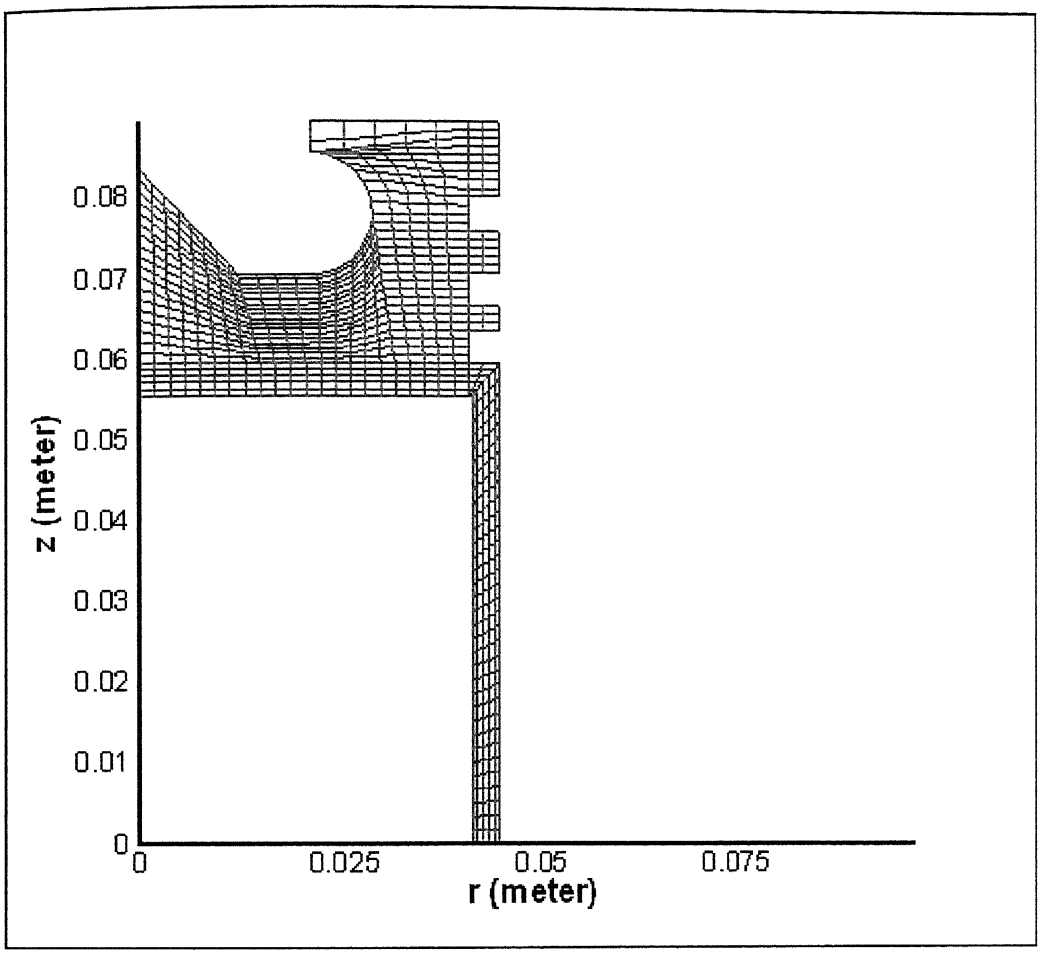

Figure 5.11: Mesh Generated Within the Half Axisymmetric Segment of the Piston.

Heat transfer coefficient at the underside of the piston, for the configuration of oil jet cooling is a function of the distance of the point under consideration from the point of impingement. Heat transfer coefficient at the underside of the piston is calculated using Steven and Webb corelation. Variation of heat transfer coefficient from the center in the radially outwards direction for the selected input parameters is shown in figure 5.12. Heat transfer coefficient at the center of the piston is approximately 340 W/m^2K, which exponentially decreases in the radi-

ally outward direction. Heat transfer coefficient near the skirt region reduces to approximately 5 W/m^2K.

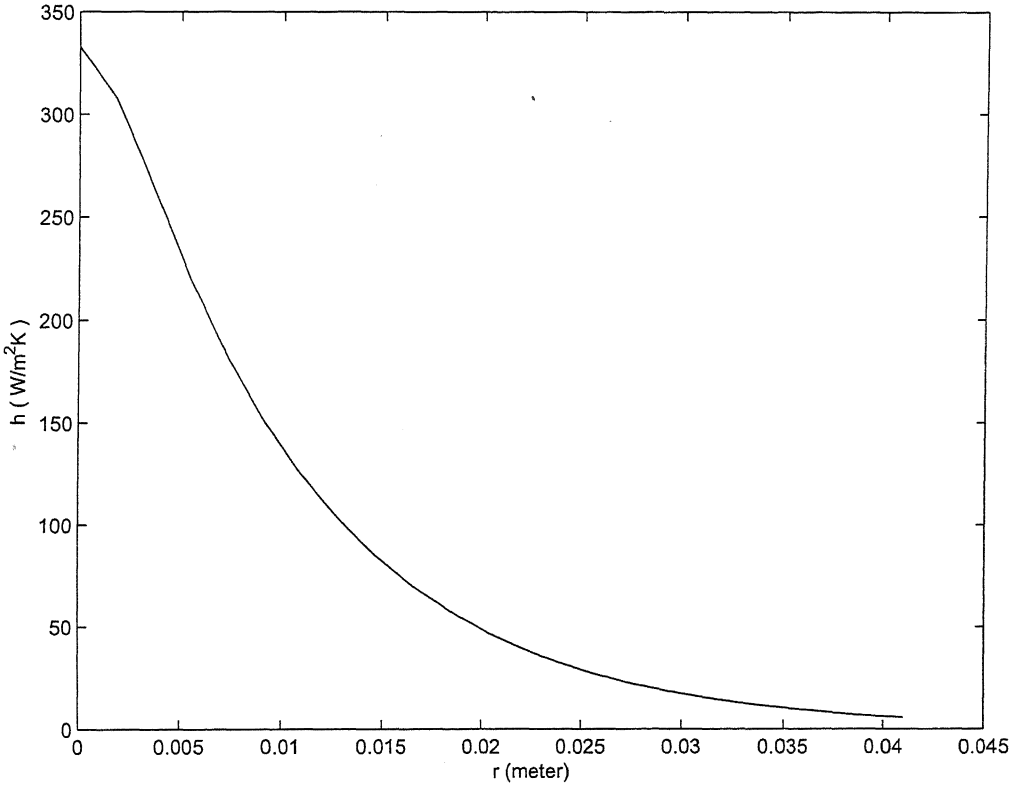

Figure 5.12: Variation of Heat Transfer Coefficient from the Center Radially Outwards

5.2.1 Piston Without/With Oil Jet Cooling with 35 kW/m^2 Heat flux

Steady state temperature profiles within half axisymmetric segment of the piston for 35 kW/m^2 heat input at the top surface of the piston and without oil jet cooling of piston is shown in figure 5.13. The maximum temperature occurs at the center of the piston top surface. The maximum temperature at the piston

top surface is approximately 280 ^{0}C. The temperature at the underside of the piston varies from 275 ^{0}C to 253 ^{0}C. The temperature in the first compression ring groove varies from 275 ^{0}C to 273 ^{0}C. The temperature in the skirt region varies from 257 ^{0}C to 223 ^{0}C.

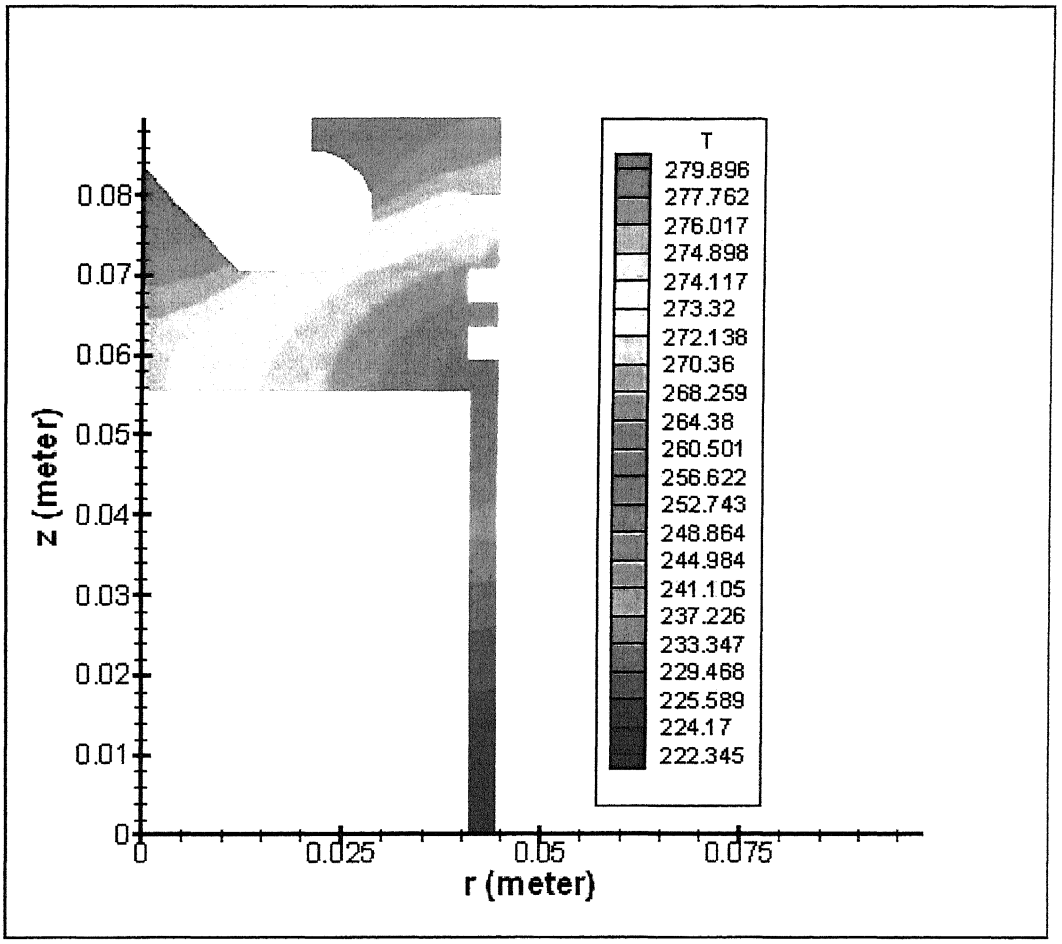

Figure 5.13: Steady State Temperature Distribution in the Piston Without Oil Jet Cooling when q" = 35 kW/m^2

Steady state temperature profiles within half axisymmetric segment of 35 kW/m^2 heat input at the top surface of the piston with other parameters remaining constant and with oil jet cooling of piston is shown in figure 5.14. The

maximum temperature occurs at the center of the piston top surface. The maximum temperature at the piston top surface is 243 ^{0}C. The temperature at the underside of the piston varies from 237 ^{0}C to 221 ^{0}C. The temperature in the first compression ring groove varies from 234 ^{0}C to 232 ^{0}C. The temperature in the skirt region varies from 221 ^{0}C to 180 ^{0}C. Here, oil jet cooling of pistons make a difference of approximately 40^{0}C all over the surface.

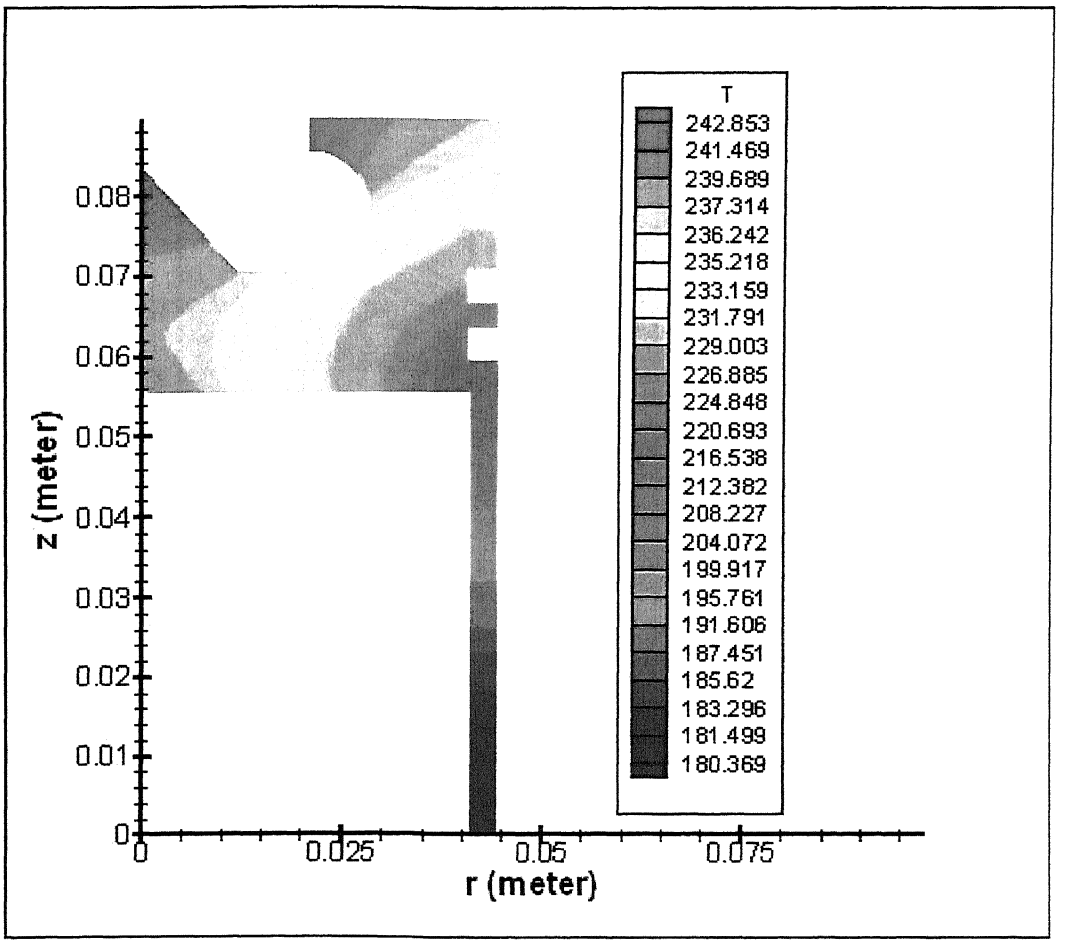

Figure 5.14: Steady State Temperature Distribution in the Piston With Oil Jet Cooling when q" = 35 kW/m^2

5.2.2 Piston Without/With Oil Jet Cooling with 40 kW/m^2 Heat flux

To understand the effect of varying power/fuel input on oil jet cooling of pistons, the normal heat input at the top surface of the piston was varied. Steady state temperature profile in half axisymmetric segment of the piston for heat input = 40 kW/m^2 heat input with other parameters remaining constant and without oil jet cooling of piston is shown in figure 5.15. The maximum temperature occurs

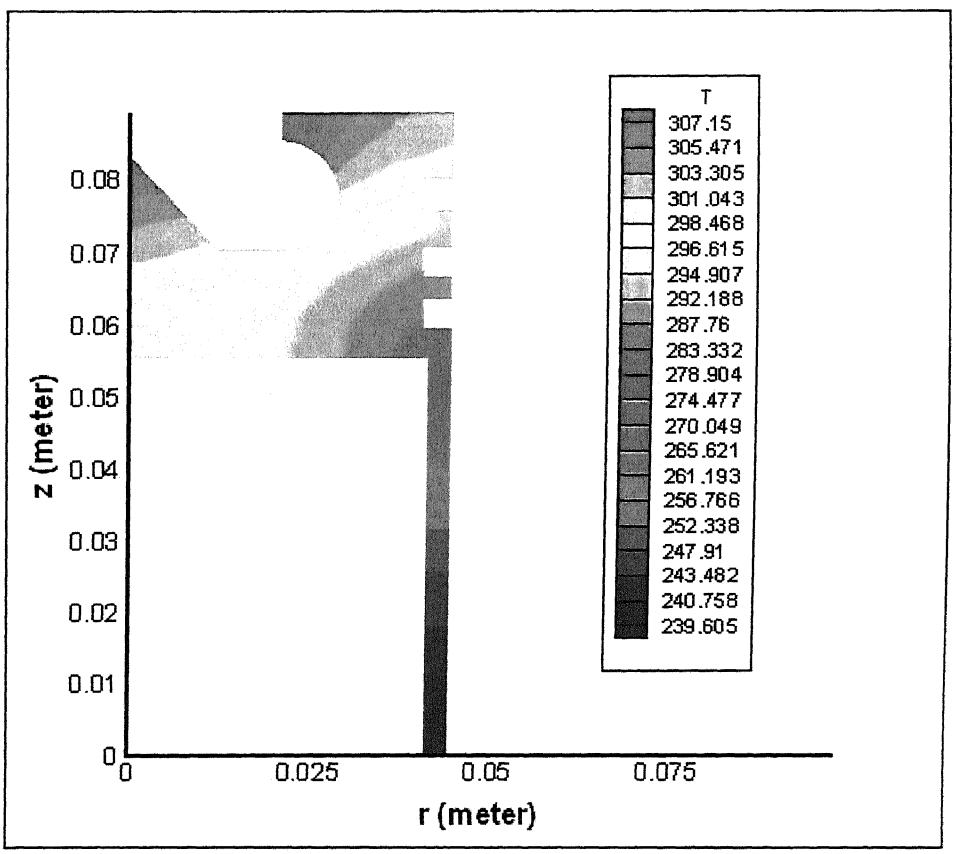

Figure 5.15: Steady State Temperature Distribution in the Piston Without Oil Jet Cooling when q" = 40 kW/m^2

at the center of the piston top surface. The maximum temperature at the piston

maximum temperature occurs at the center of the piston top surface. The maximum temperature at the piston top surface is 274^{0}C. The temperature at the underside of the piston varies from 266^{0}C to 252^{0}C. The temperature in the first compression ring groove varies from 262^{0}C to 260^{0}C. The temperature in the skirt varies from 252^{0}C to 200^{0}C. Here it can be noticed that the oil jet cooling of the pistons reduces the temperature of piston by approximately 35^{0}C all over the surface.

5.2.3 Piston Without/With Oil Jet Cooling with 45 kW/m^2 Heat flux

Steady state temperature profiles within half axisymmetric segment of the piston for the selcted input parameters without oil jet cooling of piston is shown in figure 5.17. The maximum temperature occurs at the center of the piston top surface. The maximum temperature at the piston top surface is approximately 334^{0}C. The temperature at the underside of the piston varies from 324^{0}C to 304^{0}C. The temperature in the first compression ring groove varies from 326^{0}C to 321^{0}C. The temperature in the skirt varies from 307^{0}C to 256^{0}C.

Steady state temperature profiles within half axisymmetric segment of the piston for the selected input parameters with oil jet cooling of piston is shown in figure 5.18. The maximum temperature occurs at the center of the piston top surface. The maximum temperature at the piston top surface is 302^{0}C. The temperature at the underside of the piston varies from 298^{0}C to 274^{0}C. The temperature in the first compression ring groove varies from 291^{0}C to 288^{0}C. The temperature in the skirt varies from 274^{0}C to 221^{0}C. Here it is quite evident that the oil jet cooling reduces the piston temperature by approximate 30 - 35^{0}C all over the surface.

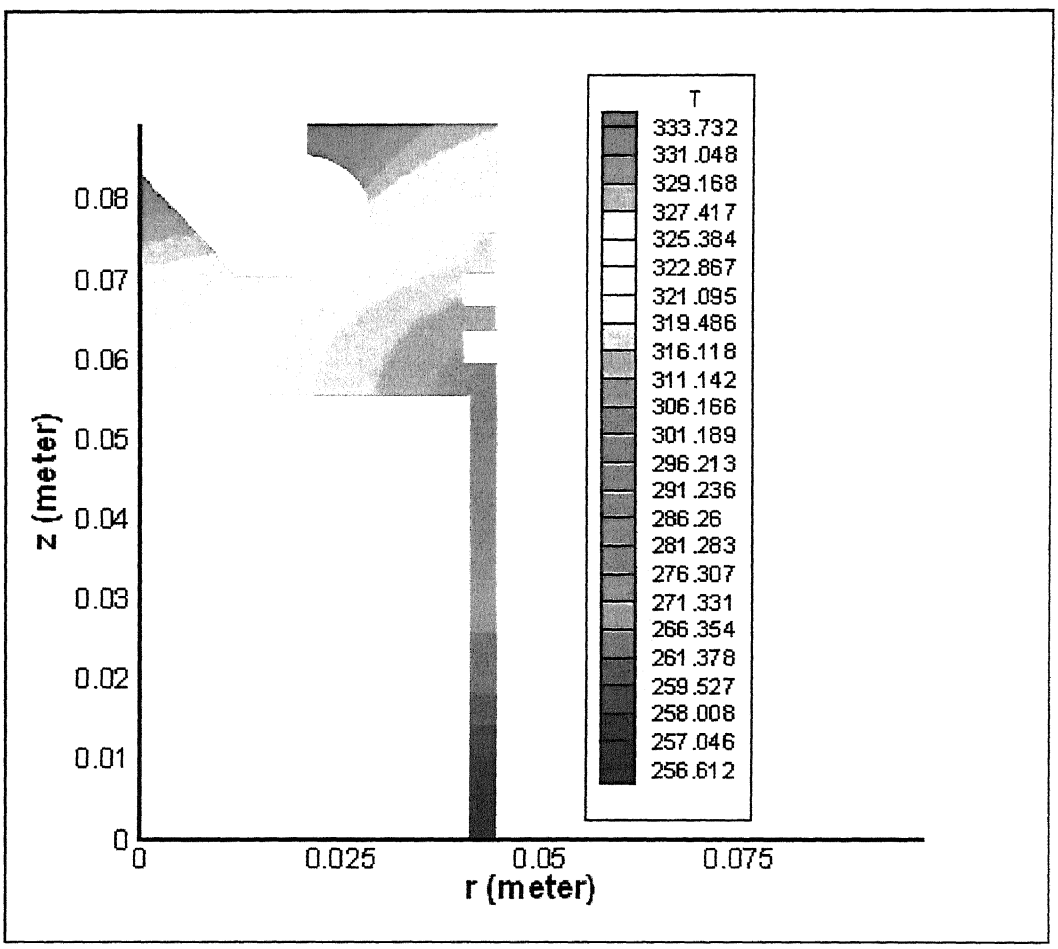

Figure 5.17: Steady State Temperature Distribution in the Piston Without Oil Jet Cooling when $q" = 45\ kW/m^2$

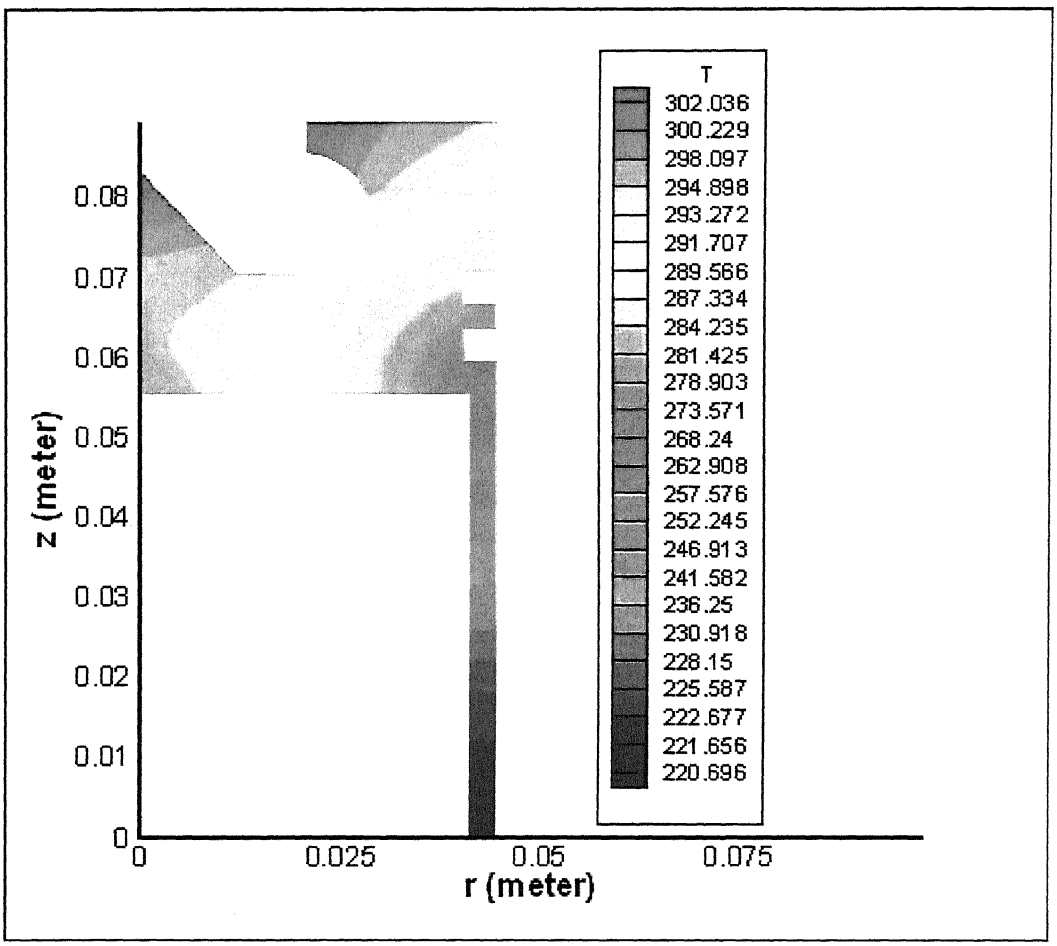

Figure 5.18: Steady State Temperature Distribution in the Piston With Oil Jet Cooling when $q'' = 45$ kW/m^2

5.2.4 Piston Without/With Oil Jet Cooling with 50 kW/m^2 Heat flux

Steady state temperature profiles within half axisymmetric segment of the piston for 50 kW/m^2 heat input at the top surface of the piston with other parameters remaining constant and without oil jet cooling of piston is shown in figure 5.19.

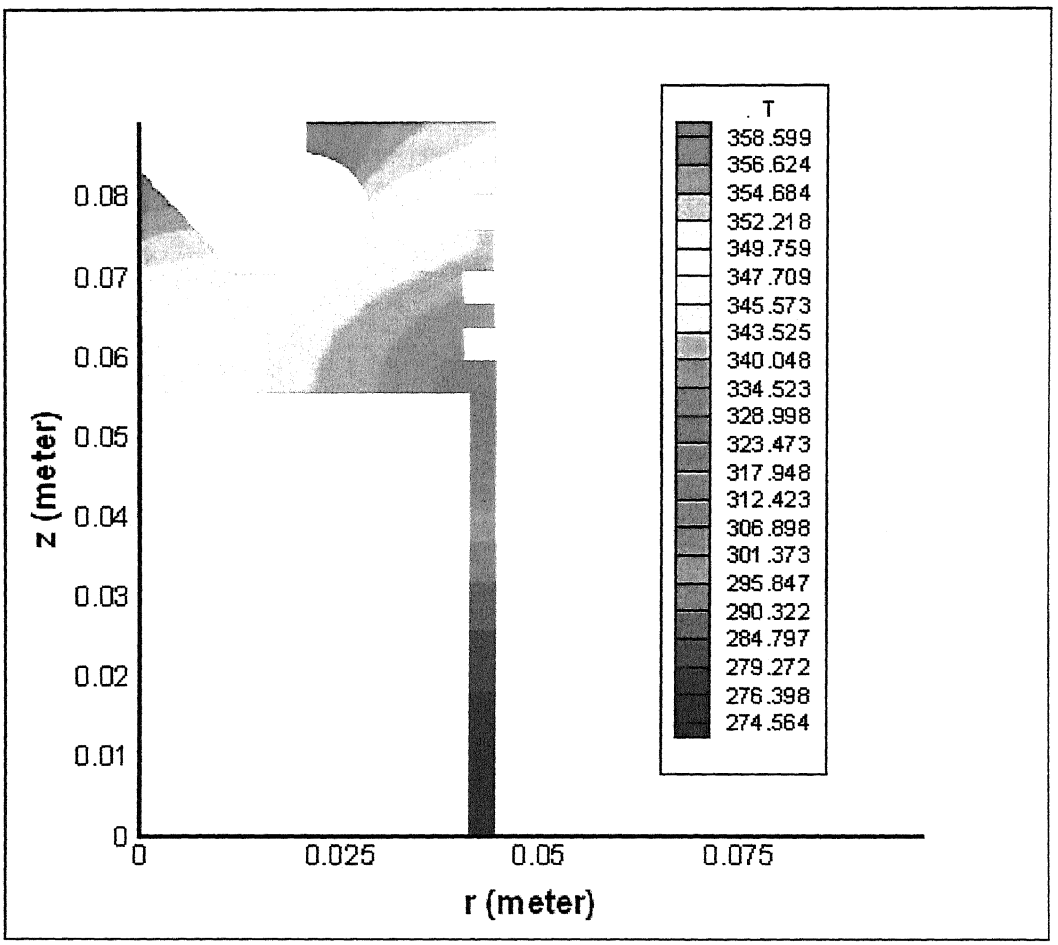

Figure 5.19: Steady State Temperature Distribution in the Piston Without Oil Jet Cooling when q" = 50 kW/m^2

The maximum temperature at the piston top surface is approximately 359^{0}C. The temperature at the underside of the piston varies from 348^{0}C to 329^{0}C. The temperature in the first compression ring groove varies from 348^{0}C to 346^{0}C. The temperature in the skirt varies from 329^{0}C to 275^{0}C.

Steady state temperature profiles in half axisymmetric segment of piston, 50 kW/m^2 heat input at the top surface of the piston with other parameters remaining constant and with oil jet cooling of piston is shown in figure 5.20. The

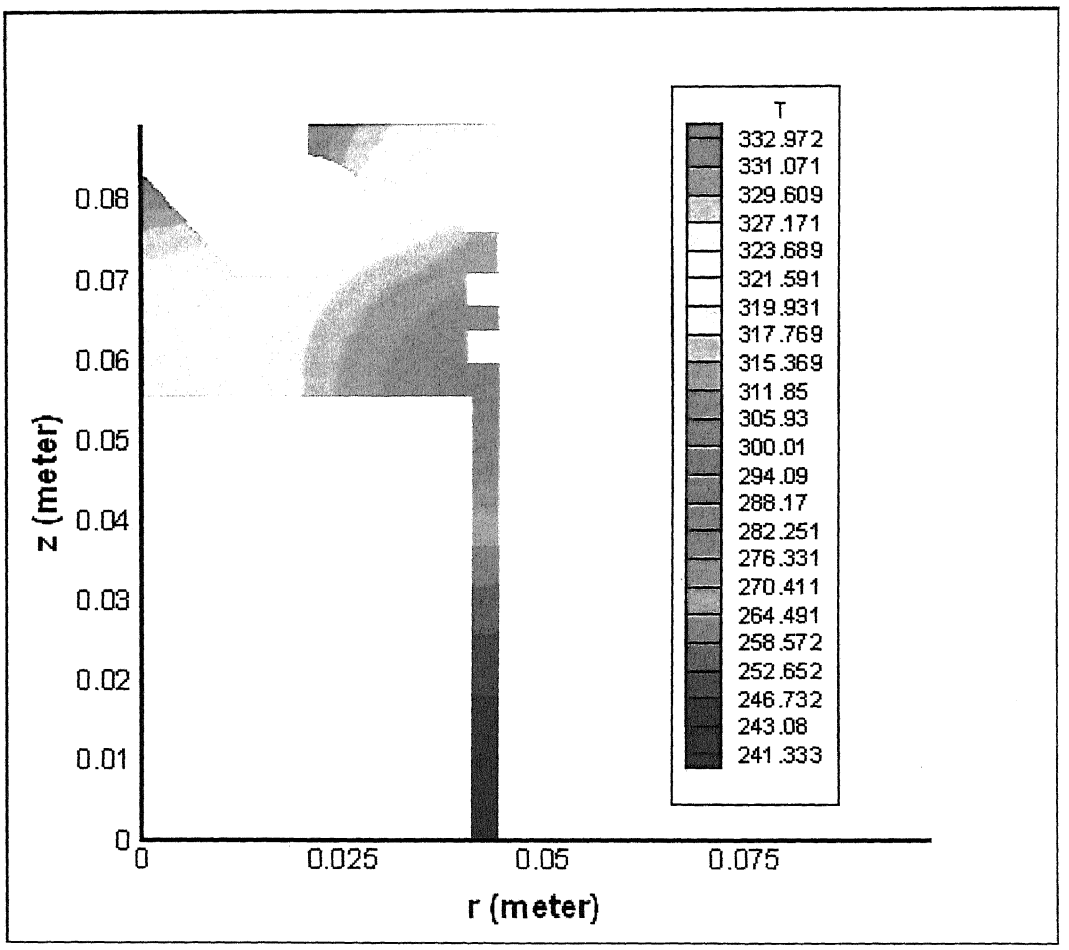

Figure 5.20: Steady State Temperature Distribution in the Piston With Oil Jet Cooling when q" = 50 kW/m^2

maximum temperature occurs at the center of the piston top surface. The maximum temperature at the piston top surface is 333 ^{0}C. The temperature at the underside of the piston varies from 324 ^{0}C to 306 ^{0}C. The temperature in the first compression ring groove varies from 315 ^{0}C to 312 ^{0}C. The temperature in the skirt varies from 306 ^{0}C to 241 ^{0}C. It is interesting to note that the oil jet cooling reduced piston temperatures in the range of 25-30^{0}C all over the surface.

Variation in maximum temperature using oil jet cooling of piston and without oil jet cooling of piston for different power densities of the engine is shown in figure 5.21. Using oil jet cooling of piston, engine power densities can be increased

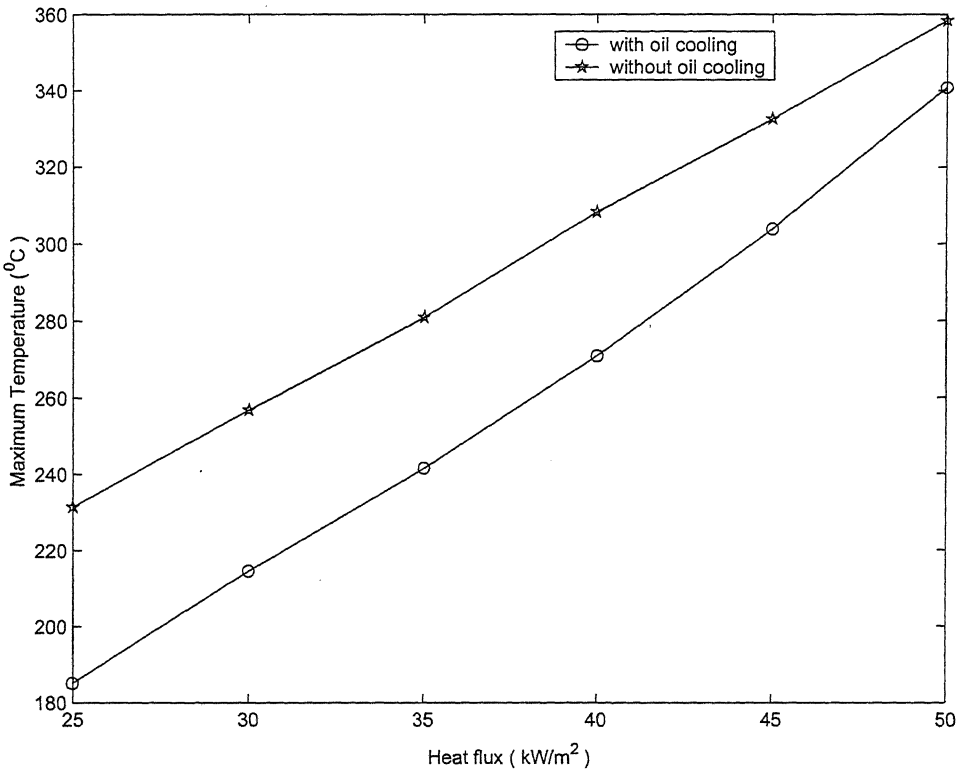

Figure 5.21: Variation in Maximum Temperatures With and Without Oil Jet Cooling for Different Engine Power Densities.

by around 10 to 12 % because of lower piston temperatures. Increase in engine power densities by 10 % is a significant increase for transportation engines, where space-weight-power ratio is of primary importance.

The temperature variation at the underside of the piston without oil jet cooling of the piston and heat input of $q" = 45$ kW/m^2, with other parameters remaining constant is shown in figure 5.22. The temperature is highest at the center of the piston and it gets lowered radially outwards towards the skirt.

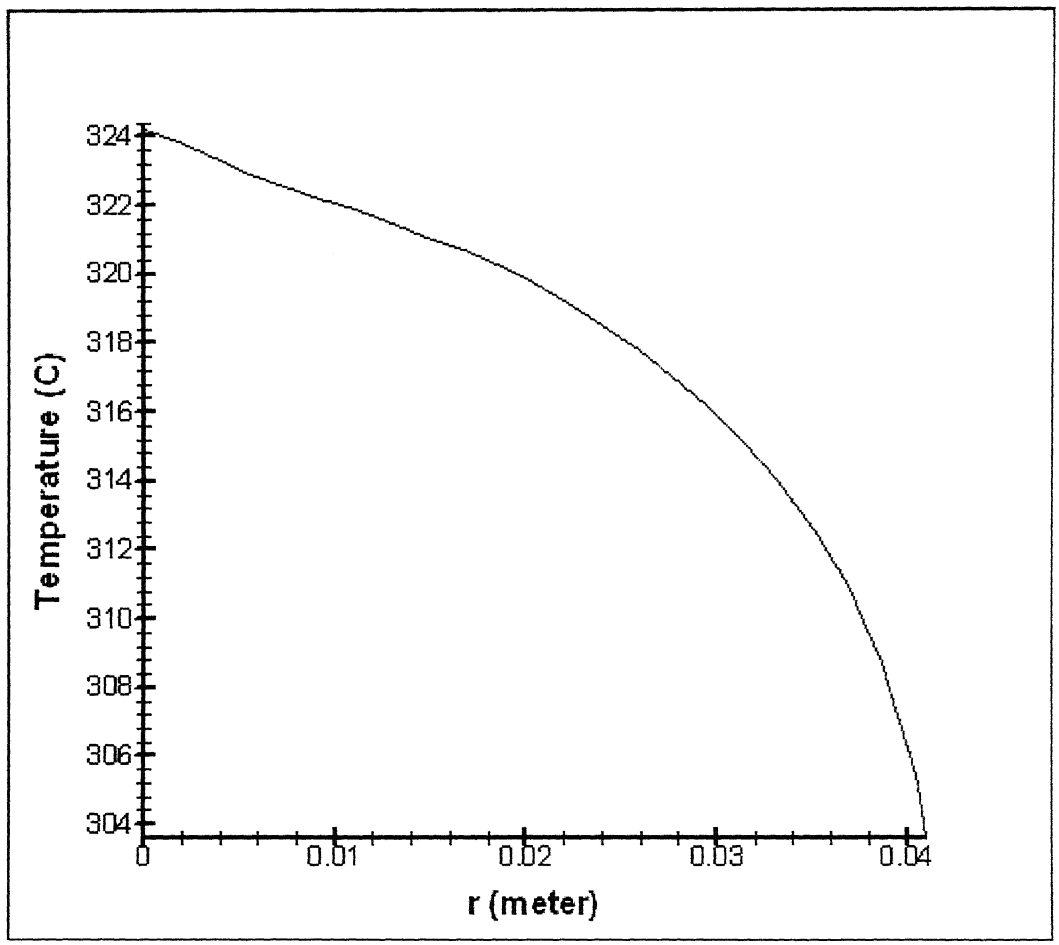

Figure 5.22: Variation in Temperature from the Center Radially Outwards Without Oil Jet Cooling.

5.2.5 Effect of Varying Nozzle Distance on Oil Jet Cooling of Pistons

The nozzle distance from the point of impingement was varied, with other parameters remaining constant and its effect on the piston temperature is examined. The heat input at the top surface of the piston is kept constant at 45 kW/m^2. The results are represented in figure 5.23. The results shows that the piston cooling gets improved with decreasing nozzle distance from the point of jet impingement.

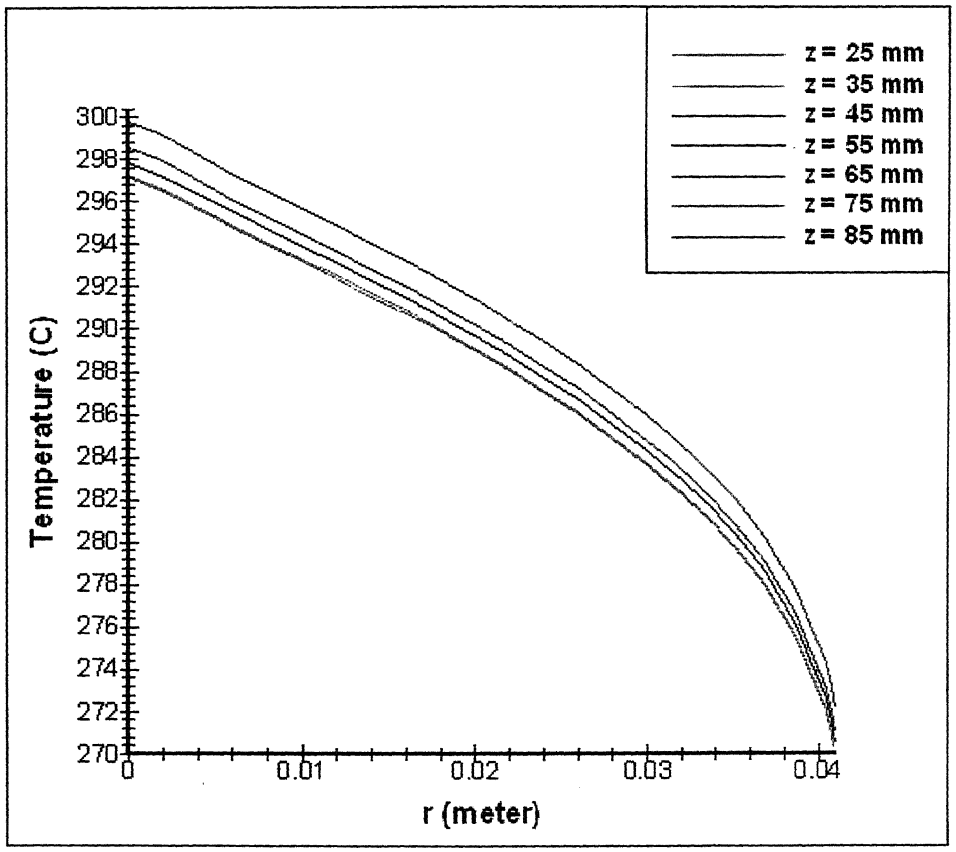

Figure 5.23: Variation in Temperature from the Center Radially Outwards for Different Nozzle Distance from the point of Jet Impingement

5.2.6 Effect of Oil Jet Velocity on Oil Jet Cooling of Piston

The effect of oil jet velocity on the piston temperature is also investigated and the results are shown in figure 5.24. The results show enhanced cooling with increasing jet velocity.

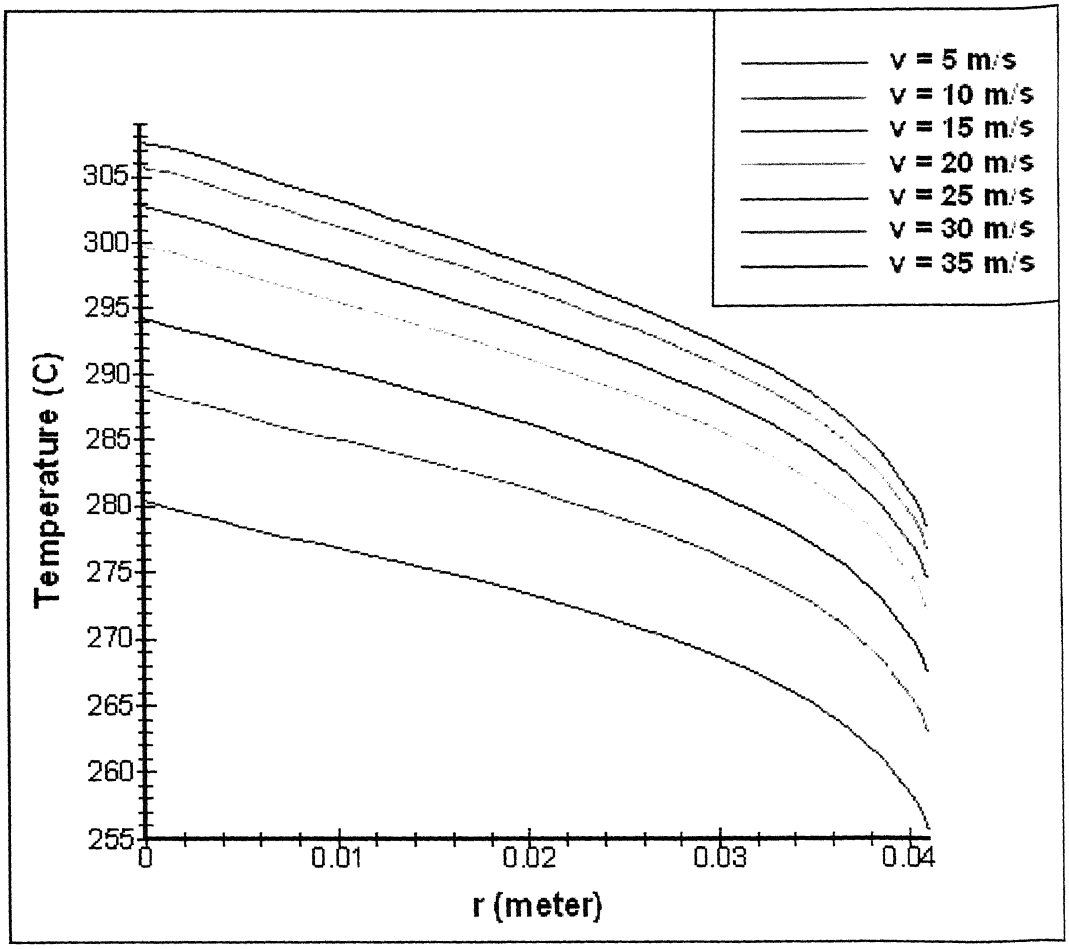

Figure 5.24: Variation in Temperature from the Center Radially Outwards for Different Relative Jet Velocity

5.2.7 Effect of Jet Diameter on Oil Jet Cooling of Pistons

The nozzle diameter was varied and its effect on the piston temperature is examined. The results are represented in figure 5.25. The result shows that the piston cooling gets improved with increasing nozzle diameter.

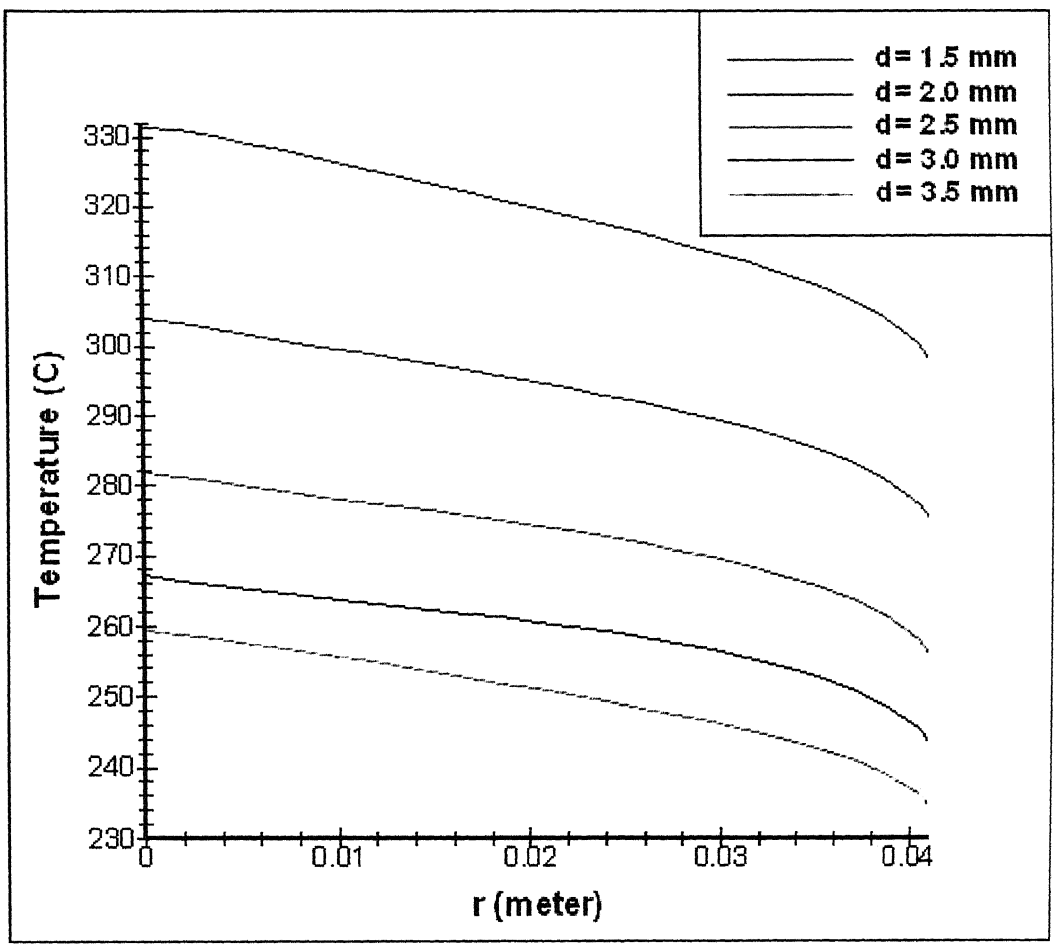

Figure 5.25: Variation in Temperature from the Center Radially Outwards for Different Nozzle Diameters.

5.2.8 Effect of Oil Type on Oil Jet Cooling on Pistons

The effect of oil type on the piston temperature is also investigated and the results are shown in figure 5.26. The results show enhanced cooling with decrease in oil viscosity.

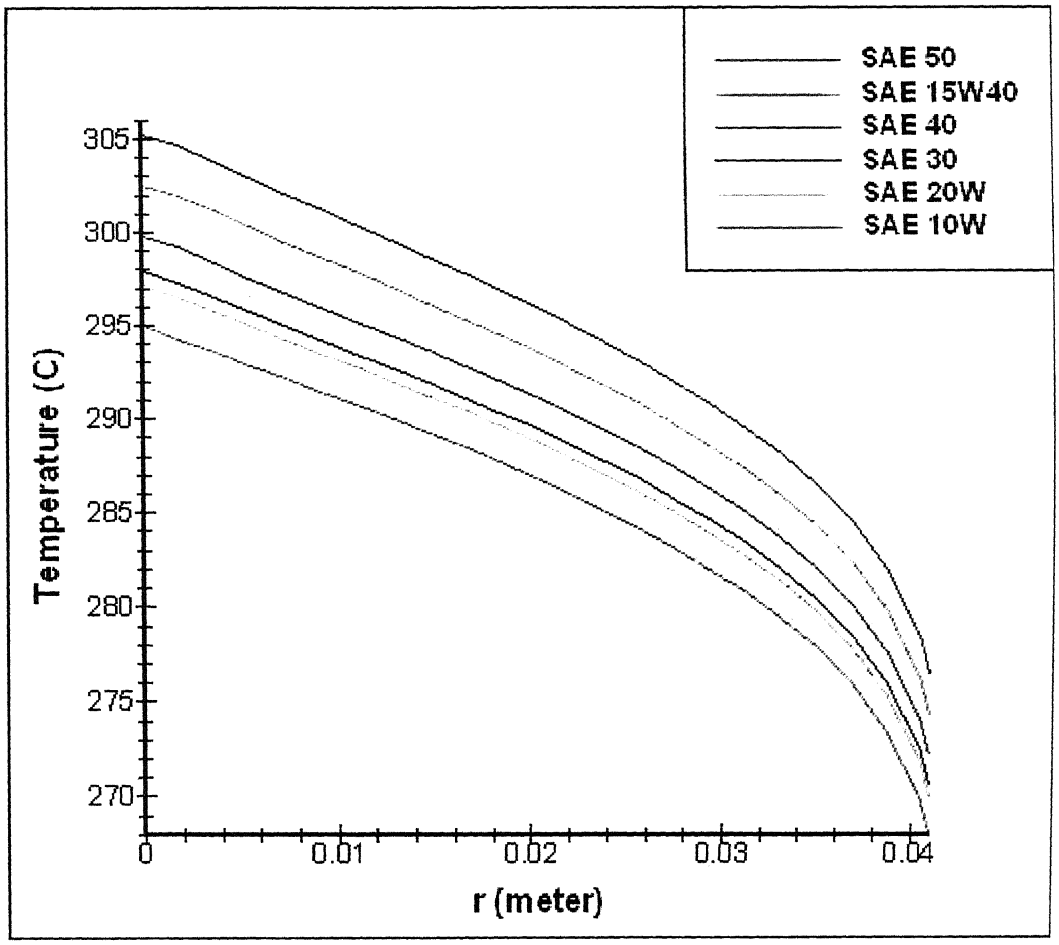

Figure 5.26: Variation in Temperature from the Center Radially Outwards for Different Oil.

5.3 Mist Generation Studies

Mist generation studies were also carried out on the flat hot plate that was used for experimental validation of the numerical simulator. Mist generated when high velocity jet striking a hot plate, were recorded using a recording web camera having a frame rate of 15 frames per second. The plate was heated upto 250^0C and oil jet was fired from below (z=85 mm) and oil jet diameter 3 mm using SAE 40 with a jet velocity of 50 m/s. As seen from figure 5.27 the oil jet was cooling the plate effectively and was not breaking.

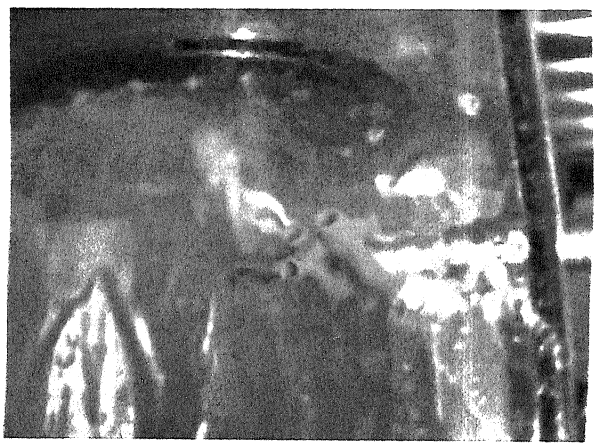

Figure 5.27: No Oil Jet Breakup from Hot Plate at 250^0C

The plate temperature was increased to 300^0C and it was observed that the oil jet was broken into bigger oil droplets after impingement on the hot plate (figure 5.28).

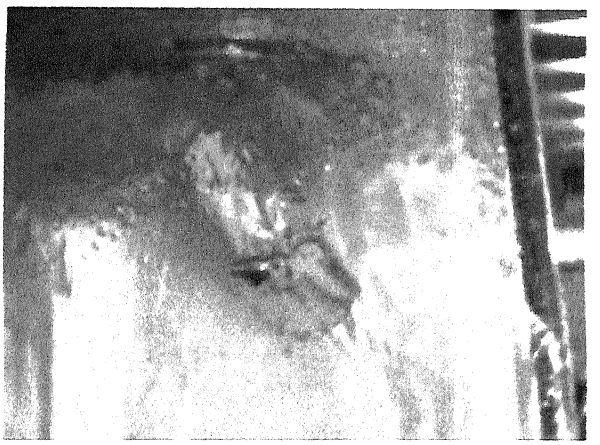

Figure 5.28: Formation of Large Size Droplets from Hot Plate at 300^{0}C.

When the jet was fired to the plate at temperature 325^{0}C, the jet started breakinginto fine droplets and localised boiling of oil at the point of impingement (figure 5.29).

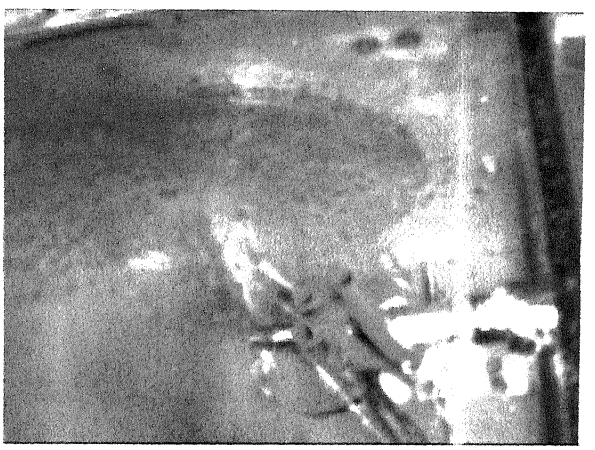

Figure 5.29: Fine Mist Generation when Hot Plate is at 325^{0}C

The temperature of the hot plate was further increased to 345^{0}C and a slightly white smoke started coming out of the impingement region along with the fine oil mist (figure 5.30).

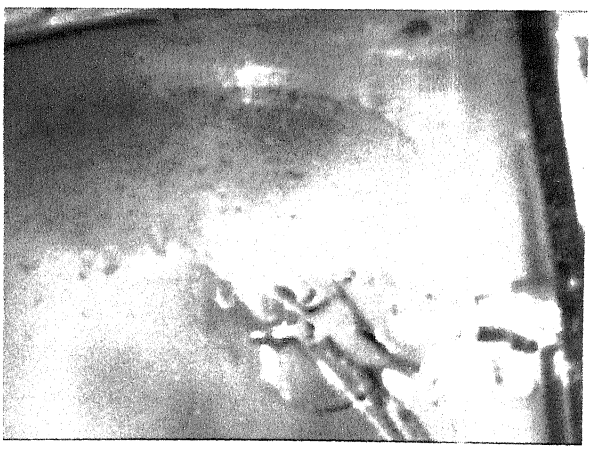

Figure 5.30: Start of Mist Generation with Smoke when Hot Plate is at 345^0C

At 355^0C, huge quantity of white smoke and oil mist was observed to be coming out of the impingement region on the hot plate

Figure 5.31: Profuse and Smoke Generation when Hot Plate is at 355^0C.

Chapter 6

Conclusion

A computational model for oil jet cooling of piston of heavy duty diesel engine was developed using Finite Element Analysis (FEA) method. Transfinite interpolation method is used for grid generation of piston geometry. Heat transfer coefficients were predicted using Steven-Webb correlation. For numerical integration Gauss-Legendre Quadrature two-point formula was used. Solution of the linear simultaneous equations was obtained by Gauss Elimination technique. For further refinement of the solution obtained by Gauss Elimination technique, Gauss-Siedel Iterative technique was used. Temperature profiles of piston are predicted. A CFD code in C language is developed for temperature prediction. The versatile CFD simulator can generate mesh for commercial grade engine pistons and predict temperature profiles with reasonable accuracy. This simulator is used for predicting temperature and effect of oil jet cooling on production grade piston. Maximum temperature on piston surface occurs at the center of the top surface of the piston. The numerical investigations of heat transfer conditions with oil jet cooling of piston have produced quantitative results of piston temperatures. An increase in power density of the engine by 10 to 12 % can be acheived by oil jet cooling of the piston.

Validation of the numerical simulator was carried out on flat plate. Average difference between numerical and experimental value is around 1.6 %. The effect of various parameters on oil jet cooling of pistons such as jet diameter, jet velocity, jet impingement distance and oil type is also investigated in details. Mist generation studies were also carried out on the flat plate using a web camera.

Oil jet cooling leads to increase in power density from the engine but it may also lead to increase in non-tail pipe unburnt hydrocarbon emissions, which are not easy to detect/measure. Hence it is extremely important to avoid the piston temperature, where the mist generation with smoke starts.

Chapter 7

Future Scope of Work

1. Experimental validation of the numerical simulator for piston should be carried out using existing experimental setup with a heated piston. Heating arrangement for the piston is already manufactured. Piston with the heating arrangement is shown n figure 7.1. Infrared thermal imaging camera may be

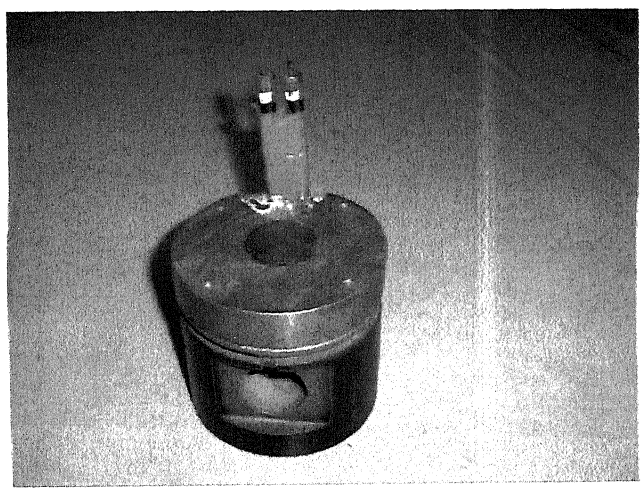

Figure 7.1: Piston with Heating Arrangement

used to capture the temperature profile of the piston.

2. Further experimental studies should be carried out on an optical engine to

precisely know the heat flux input at several location on the top surface of the piston.

3. In the numerical simulator, the heat input at the top side of the piston is taken as roughly 1 % of the power density of the engine (based on the literature). Actual modeling of the combustion phenomenon may be carried out to know the amount of heat input at the top surface of the piston and experimental studies may be carried out to find the amount of heat input at the top surface of the piston.

Appendix A

Structured Grid Generation Techniques

The techniques available for generating structured grids can be divided into three major categories. These are:

1. algebraic methods
2. conformal mapping and
3. methods using partial differential equations.

Among these procedures, algebraic grid generation is efficient and it can be applied to two dimensional as well as three dimensional geometries. Some explicit control of grid spacing is also possible. However, slope dicontinuities present at the boundaries tend to propogate to the interior and in such cases, the grid suffers from lack of smoothness. Conformal mapping provides a smooth orthogonal grid except at a few singular points, though its applicability to three dimensional problems is rather limited. Partial differential equation based methods generate grids which exhibit a good compromise between the various desired grid properties. They have a wide

range of applicability. But the implementation of PDE-based grid generation is cumbersome and time consuming. Here only algebraic grid generatio method for the generation of structured grids is described.

A.0.1 Algebraic Grid Generation

A more general procedure for the algebraic generation of grids is based on interpolation. Coordinates of the interior nodes are obtained by interpolation between the prescribed boundary data. In algebraic methods, the transformation can be done analytically when the boundaries are regular. On the other hand, if the boundary is highly irregular and complex, the domain transformation is carried out numerically using suitable interpolation procedures. A very useful technique for this purpose is the Transfinite Interpolation, which is illustrated in the following example.

Consider the four sided geometry (ABCD) (figure A.1(a)). It is desired to generate ξ-constant and η-constant lines within ABCD which upon transformation would become equi-spaced orthogonal grid lines inside a rectangular domain of size of 1 x 1. The first task to be completed is the placement of grid points on the boundary (figure A.1(b)); here, in order to get a rectangular grid, the number of points on opposite sides should be equal. Also, if some idea is available regarding the nature of gradients in the problem, the boundary points can be located so as to resolve the high gradient regions. Now, let us apply linear interpolation in the ξ-direction between two grid points which lie on the same η = constant line. Since the total range of ξ variation is from 0 to 1, the linear interpolation formulae for

the coordinates of an interior point P are written as

$$\begin{aligned} x_p^{'} &= (1-\xi)x_E + \xi x_F \\ y_p^{'} &= (1-\xi)y_E + \xi y_F \end{aligned} \tag{A.1}$$

where E and F are the two boundary grid points. Carrying out the same operation for all the η-constant lines including the boundaries ($\eta = 0$ and $\eta = 1$) the interpolated points (marked by x) will appear as in figure A.1(c). It may be noted that on the boundaries AB and CD, the grid points obtained by unidirectional interpolation between the coordinates of the corner nodes (A, B) or (C, D), do not coincide with the actual grid points shown as dots (.). In order to remove this anomaly, the difference between the actual points and the interpolated points should be subtracted on the $\eta = 0$ and $\eta = 1$ boundary curves. Moreover, some corrections need to be applied to the coordinates of point P which have been obtained by unidirectional interpolation in the ξ-direction, along an η = constant line. Introducing such corrections brings in the influence of the boundary grid point data in the η-direction also, for determining the coordinates of point P. Considering two grid points G and H corresponding to the ξ = constant line on which P lies, the corrections for the coordinates of point P are

$$\begin{aligned} \triangle x_P &= (1-\eta)\triangle x_G + \eta \triangle x_H \\ \triangle y_P &= (1-\eta)\triangle y_G + \eta \triangle y_H \end{aligned} \tag{A.2}$$

where $\triangle x_G$, $\triangle x_H$, $\triangle y_G$ and $\triangle y_H$, are the corrections for the boundary points given

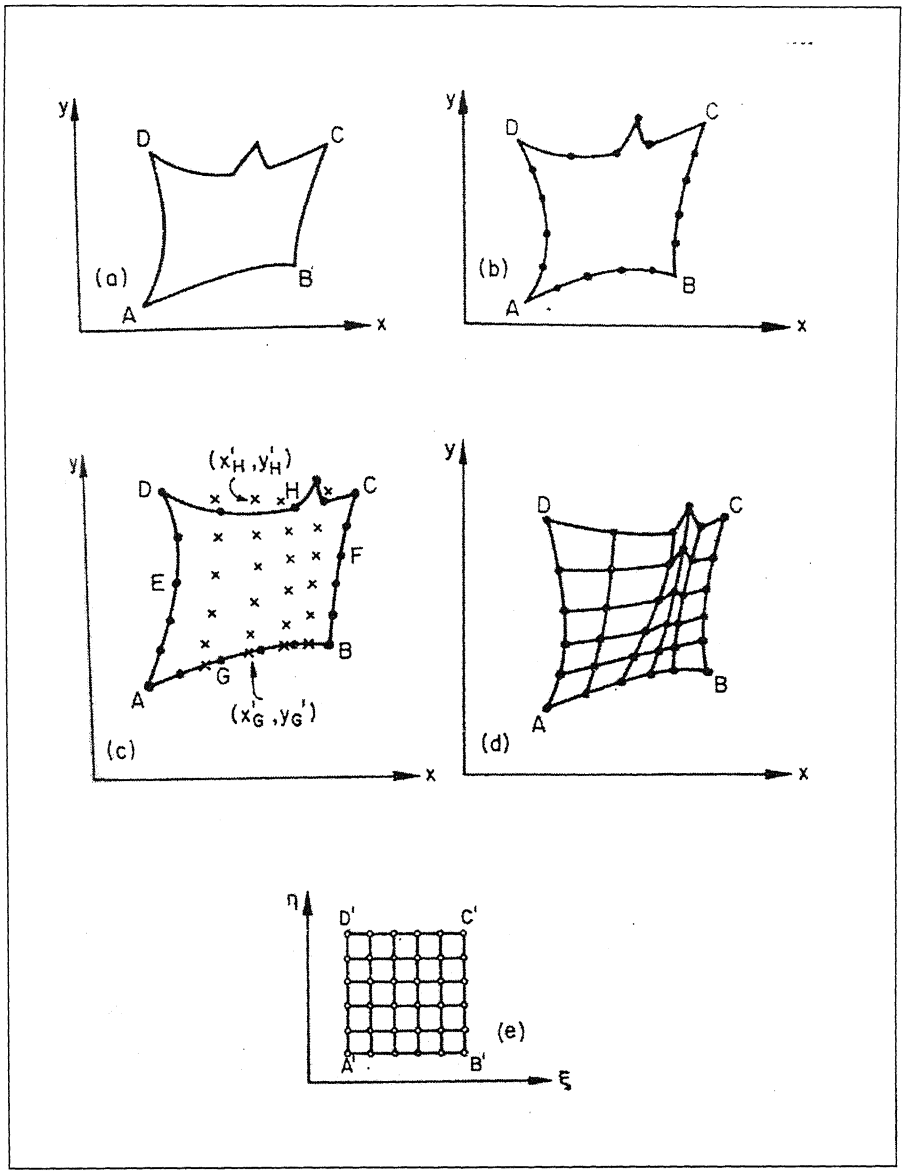

Figure A.1: Transfinite Interpolation.

by

$$\begin{aligned}
\triangle x_G &= x'_G - x_G \\
\triangle y_G &= y'_G - y_G \\
\triangle x_H &= x'_H - x_H \\
\triangle y_H &= y'_H - y_H
\end{aligned} \tag{A.3}$$

In equation A.3, the coordinates indicated with prime are those obtained by unidirectional interpolation in ξ- direction and those without prime are the actual boundary grid point data. The final values of the coordinates of P (after interpolation in both ξ and η directions) are obtained as

$$\begin{aligned} x_P &= x_P^{'} - \triangle x_P \\ y_P &= y_P^{'} - \triangle y_P \end{aligned} \tag{A.4}$$

Performing the above sequence of operations for every interior point gives the mesh in the physical domain as shown in figure A.1(d). The corresponding transformed mesh is shown in figure A.1(e).

It is important to note that unidirectional interpolation can be done first in the η direction along each ξ = constant curve. In that case, corrections will have to be applied for matching actual grid points and the interpolated points along the boundaries AD ($\xi = 0$) and BC ($\xi = 1$). The final grid obtained by both the above approaches will be exactly same. The general algorithm of transfinite interpolation, can therefore, be stated as:

1. Place grid points on the boundaries of the domain as desired

2. Apply unidirectional interpolation in ξ-direction (or η-direction) between the boundary grid data given on the curves $\xi = 0$ and $\xi = 1$ (or $\eta = 0$ and $\eta = 1$) and obtain the coordinates $x_P^{'}$, $y_P^{'}$ for every interior and boundary point.

3. Calculate the mismatch between the interpolated and the actual coordinates on the $\eta = 0$ and $\eta = 1$ (or $\xi = 0$ and $\xi = 1$) boundaries.

4. Linearily interpolate the difference in the boundary point coordinates and find the correction to be applied to the coordinates of every interior point.

5. For each point, final coordinate value is equal to unidirectionally interpolated value - correction.

The transfinite interpolation described above is a very simple and powerful numerical procedure. It can be applied to two dimensional as well as three dimensional situations and for all grid configurations (O-type, C-type, H-type etc.). The main weakness of this procedure is that the slope discontinuities at the boundary propogate to the interior and spoil grid smoothness. However, since the metric derivatives are also evaluated numerically, the effect of a slope dicontinuity is not severe, as in the case of analytical transformation.

Appendix B

Code Information

First run the program 'meshgen.c'. The input parameters required for this program are the number of grids into which the domain has to be divided in r and z directions. This program has a function by the name meshgen, which uses Transfinite Interpolation method to generate mesh within the specified domain. In the main program part of 'meshgen.c' the domain profile is specified. Users will have to change the profile if they require to generate a mesh within other piston. The coordinates of the points are written in a file 'mesh.dat'. Users can view the mesh generated within the profile using plotting softwares like GNUPLOT or Tecplot.

Next run the program 'coordinate.c'. This file takes 'mesh.dat' written by 'meshgen.c' as input and arranges the coordinates in a sequential order as per their global positioning. The coordinates of the points arranged in a sequential manner according to their global positioning are written in a file 'coordinate.dat'.

Next run the program 'conmatrix.c'. This program produces the connectivity matrix for all the global elements within the domain. The output of this program is written in a file 'conmatrix.dat'.

Next run the program 'Kmatrix.c'. This program takes 'coordinate.dat'

and 'conmatrix.dat' as input files. It also requires conductivity of the material as input parameters. This program then calculates the K matrix taking the above mentioned parameters. The calculated values of the K matrix are written in a file 'Kmatrix.dat'. Only non-zero elements of the calculated K matrix are written in the file. As only non-zero elements are written in the file, this file has three columns. First column of the file 'Kmatrix.dat' indicates the row number of the element in the K matrix. Second column of the file 'Kmatrix.dat' indicates the column number of the element in the K matrix. Third column of the file 'Kmatrix.dat' indicates the value of the entry in the K matrix.

Next run the program 'Hmatrix.c'. This program also, similar to 'Kmatrix.c' takes 'coordinate.dat' and 'conmatrix.dat' as input files. In addition, it also requires the properties of oil as input parameters. The properties of oil required are thermal conductivity of oil, specific heat of the oil at constant pressure (C_p), kinematic viscosity of the oil and density of the oil. This program also requires as input parameters the diameter of the nozzle used for oil jet cooling of piston, relative velocity of the jet and vertical distance of the piston underside fron the nozzle. It also requires as input parameters the heat transfer coefficient of water cooling the cylinder liner surface. From the literatures, it is found that the heat transfer coefficient of the water cooling the cylinder liner surface is 80 W/m^2K. Using the above parameters as input, this program calculates the H matrix. As in the case of K matrix only non-zero elements are written in a file 'Hmatrix.dat'. 'Hmatrix.dat' also has three columns. First column indicates the row number of the element in the H matrix, whereas the second column indicates the column number of the element in the H matrix and the third column indicates the value of the entry in the H matrix.

Next run the program 'kphmatrix.c'. This program takes 'Kma-

trix.dat' and 'Hmatrix.dat' as input files and performs matrix addition of the K matrix and H matrix. The output of this program is written in a file 'kphmatrix.dat'.

Next run the program 'Pmatrix.c'. This program also takes 'coordinate.dat' and 'conmatrix.dat' as input files. In addition, it requires as input parameters the temperature of cooling water and temperature of cooling oil. From the literature, it is found that the temperature of cooling water is around 72 ^{0}C. The calculated value of the P matrix is written in a file 'Pmatrix.dat'.

Next run the program 'Qmatrix.c'. This program also takes 'coordiante.dat' and 'conmatrix.dat' as input files. In addition, it requires as input parameters the normal heat input at the top surface of the piston. The calculated value of the Q matrix is written in a file 'Qmatrix.dat'.

Next run the program 'QpP.c'. This program takes 'Pmatrix.dat' and 'Qmatrix.dat' as input files and performs matrix addition of the Q matrix and P matrix. The output of this program is written in a file 'QpP.dat'.

To solve the linear simultaneous equations Gauss elimination technique is used. Matlabs inbuilt function, to find the solution of linear simultaneous equations is used. Run the m file 'tempre.m' in Matlab. The output of the m file is written in a file 'tempre.dat'.

Next run the program 'temp.c'. It is necessary to run this program because it arranges the coordinates of the points and temperatures of the points in a way which is suitable to plot, especially the contours. The output of this file is written in 6 files namely 'temp1.dat', 'temp2.dat', 'temp3.dat', 'temp4.dat', 'temp5.dat' and 'temp6.dat'. Any plotting software which is capable of plotting contours can be used for viewing the contours.

If further refinement of the solution is required then run the program

'tempini.c'. This program uses Gauss Siedel iterative technique to refine the solution. After running this program again run the program 'temp.c'.

To obtain the temperature profiles within the piston without oil jet cooling of piston, run all the programs upto 'Kmatrix.c'. Then run the program 'Hmatrixwtc.c'. Then run the program 'kplush.c'. Then carry out all the sequences mentioned above.

Appendix C

Properties Chart

C.1 Thermal Conductivities of Materials Used in Study

Thermal conductivity of Aluminum alloy = 137 W/mK

Thermal conductivity of Mild Steel = 54 W/mK

C.2 Properties of Oils

SAE GRADE	10W	20W	30	40	15W-40	50
Specific gravity @ 15.6 ^{0}C	0.876	0.879	0.886	0.897	0.882	0.896
Kinematic viscosity @ 70 ^{0}C, cSt	6.5	8.8	11.9	14.5	15.5	18.0
C_p, J/kgK	2219	2219	2219	2219	2219	2219
Thermal conductivity, W/mK	0.137	0.137	0.137	0.137	0.137	0.137

Bibliography

[1] Ferguson C. R. and Kirpatrick A. T. *Internal Combustion Engines.* John Wiley & Sons Inc., 2001.

[2] http://hadmac.com/piston_&liner.htm.

[3] Eugene J. Manganiello. Piston temperatures in an air-cooled engine for various operating conditions. Technical Report 698, NACA.

[4] http://www.marinediesels.info.

[5] http://www.elsbett.com/gd/eteche.htm.

[6] Dhariwal H. C. Control of blowby emissions and lubricating oil consumption in ic engines. *Energy Convers. Mgmt*, 38(10–13):1267–1274, 1997.

[7] Martin H. Heat and mass transfer between impingement gas jets and solid surfaces. In Hartnett J. P. and Irvine Jr. T. I., editors, *Advances in Heat Transfer*, volume 13, pages 1–60, 1977.

[8] Down S. J. and James E. H. Jet impingement heat transfer - a literature survey. *ASME Paper 87 - HT - 35*, 1987.

[9] Hrycak P. Heat transfer from impingement jets to a flat plate. *International Journal of Heat and Mass Transfer*, 26:1857–1865, 1988.

[10] Beltaos S. Oblique impingement of circular turbulent jets. *Journal of Hydraulic Research*, 14:17–36, 1976.

[11] Sparrow E. M. and Lovell B. J. Heat transfer characteristics of an obliquely impinging circular jet. *Journal of Heat Transfer, Transcations of ASME*, 102, May 1980.

[12] Chang H. Oh, John H. Lienhard, Hesham F. Younis, Rudy S. Dabhura, and Dirk Michels. Liquid jet-array cooling modules for high fluxes. *AIche Journal of Fluid Mechanics and transport Phenomenon*, 44(4):769–779, Apr. 1998.

[13] Mao-Yu Wen and Kuen-Jang Jang. An impingement cooling on a flat surface by using circular jet with longitudinal swirling strips. *International Journal of Heat and Mass Transfer*, pages 1–12, 2003.

[14] Oliphant K., Webb B. W., and Mcquay M. Q. An experimental comparison of liquid jet array and spray impingement cooling in the non-boiling regime, 1998.

[15] Cristina Cornaro, Amy S. Fleischer, Michael Rounds, and Richard J. Goldstein. Jet impingement cooling of a covex semi-cylindrical surface, 2001.

[16] Steven J. and Webb B. W. The effect of inclination on local heat transfer under an axisymmetric, free liquid jet. *International Journal of Heat Transfer*, 34(4/5):1227–1236, 1991.

[17] Stevens J. and Webb B. W. Local heat transfer coefficient under and axisymmetric, single-phase liquid jet. *ASME Journal of Heat Transfer*, 113:71–78, 1991.

[18] Bush J. E. Heat transfer in a reciprocating hollow piston partially filled with a liquid. Technical Report 51, Stanford University, 1961.

[19] Bush J. E. and London A. L. Desin data for cocktail shaker cooled pistons and valves. *SAE-650727*, 1965.

[20] French C. C. J. Piston cooling. *SAE-720024*, 1972.

[21] Evans C. A. Cocktail shaker. *Heat Transfer Science Library, University of Nottingham*, 1977.

[22] Hidehiko Kajiwara, Yukihiro Fujioka, Tatsuya Suzuki, and Hideo Negishi. An analytical approach for prediction of piston temperature distribution in diesel engines. *JSAE Review*, 23:429–434, 2002.

[23] Jos, Martins Leites M., and Roberto De Camargo C. Articulated piston cooling optimization. *SAE-930276*, 1993.

[24] Marcos M. Pimenta and Escola Politécnica da USP. Cooling of automotive pistons: Study of liquid-cooling jets. *SAE-931622*, 1993.

[25] Stotter A. Heat transfer in piston cooling. *SAE-660757*, pages 705–710, 1967.

[26] Flynn, Gregory Jr., Underwood, and Arthur F. Adequate piston cooling - oil cooling as a means of piston temperature control. *SAE*, 53(2):120–128, Feb. 1945.

[27] Otto Kruggel. Calculation and measuring of piston temperatures of air-cooled two-stroke gasoline engines. *SAE-710578*, pages 1911–1929, 1971.

[28] Gerhard Woschni and Johann Fieger. Determination of local heat transfer coefficients at the piston of a high speed diesel engine by evaluation of measured temperature distribution. *SAE-790834*, pages 2807–2815, 1979.

[29] Huebotter H. A. and Young G. A. Flow of heat in pistons. *Bull. No. 25, Purdue University. Eng. Exp. Station Bull.*, IX(12), Dec. 1925.

[30] Janeway R. N. Quantitative analysis of heat transfer in engines. *SAE*, 43(3):371–380, Sept. 1938.

[31] Paschkis, Victor, and Baker H. D. A method for determining unsteady state heat transfer by means of an electrical analogy. *Journal of Heat Transfer, Transactions of ASME*, 64(2):105–112, Feb. 1942.

[32] Willis E. J. and Anderson R. G. Operating temperatures and stresses in aluminum aircraft engine parts. *SAE*, 52(1):28–36, Jan. 1944.

[33] Sanders J. C. Analysis of variation of piston temperature with piston dimensions and undercrown cooling. Technical Report 895, NACA.

[34] Baker H. and Wright. A study of piston temperature and their relation to piston design. *Proc. Inst. Auto. Engg. (London)*, 27:109–138, Nov. 1932.

[35] Wang Q., Cao Y., Wang R., Mignano F., and Chen G. Studies of a heat-pipe cooled piston crown. *Transactions of the ASME, Journal of Engineering for Gas Turbines and Power*, 122:99–105, 2002.

[36] Mani Bijoy Varghese and Avinash Kumar Agarwal. Numerical investigations of piston cooling using oil jet. In *Third International Conference on Synergy of Fuel and Automotive Technology for Cleaner Environment*, number SAE-2004-28-0061, 2004.

[37] Ghoshdastidar P. S. *Computer Simulation of Flow and Heat Transfer.* Tata McGraw-Hill Publication, 2003.

[38] Ganesan V. *Internal Combustion Engines.* Tata McGraw-Hill Publishing Co., New Delhi, 2^{nd} edition, 2003.

[39] Doughtie and Venton Levy. *Elements of Mechanism.* John Wiley & Sons, New York, 1954.

[40] Reddy J. N. *An Introduction to the Finite Element Method.* Tata McGraw-Hill Publishing Co., New Delhi, 2^{nd} edition, 2003.

[41] William H. Press, Saul A. Teukolsky, William T. Vetterling, and Brian P. Flannery. *Numerical Recipes in C, The Art of Scientific Computing.* Cambridge University Press, 2^{nd} edition, 1992.

[42] Muralidhar K. and Sundararajan T. *Computational Fluid Flow and Heat Transfer.* Narosa Publishing House, 1995.

[43] Ferziger J. H. and Perić M. *Computational Methods for Fluid Dynamics.* Springer-Verlag, 3^{rd} edition, 2002.

[44] Holman J. P. *Heat Transfer.* Tata McGraw-Hill Publishing Co., New Delhi, 8^{th} SI metric edition, 2002.